Celestial Mechanics and Dynamical Astronomy (2025) 137:37
https://doi.org/10.1007/s10569-025-10267-x

RESEARCH

On Ganymede's synchronous rotation in the presence of a subsurface ocean

Christoph Lhotka[1] · Giuseppe Pucacco[1] · Matteo Veglianti[1]

Received: 9 May 2025 / Revised: 21 October 2025 / Accepted: 30 October 2025 /
Published online: 15 November 2025

Abstract
We investigate the librations of Ganymede's core and shell on different time scales around its synchronous spin-orbit resonant state. Our study is based on dynamical models of the moon being composed of a thin external shell and an inner solid core, separated by a potential internal ocean. Here, we assume that the two layers are interacting via a gravitational torque and a viscous torque. External tidal torques on each layer are also considered. We derive and analyze the fundamental equations of motion using analytical and numerical methods for initial conditions close to resonance and several parameters. A core subject of our study is to provide estimates of the damping time scales for the free librations and the geometry of the dynamical attractor in phase space. In addition, we analyze the separate torques, i.e., their isolated effects on the short- and mid-term evolution. We derive explicit solutions that enable us to perform an accurate investigation of the system parameters, i.e., their influence on the amplitudes and frequencies. Analytical estimates of the damping time scales are provided on the basis of the real parts of the eigenvalues and are validated by numerical simulations. Finally, we test our findings, being based on a well-established class of dynamical models, also with an alternative approach based on creep tide theory. On the basis of this model we provide relaxation time scales of the elastic layers and compare the different dynamical phases with the model based on rigid layers. With this we are able to provide a plausible range of damping time scales (ranging from 3 to 100 years), relaxation factors (ranging from 0.5 to 30 years) libration amplitudes of the damped solutions (15 m), and periods of the damped solutions (7.2 days). Our study enables us to constrain the order of magnitudes of the parameters that describe the composition of the layers, their rheological properties, and the current dynamical state of Ganymede being consistent with mid-term simulations. This work may serve as a framework for the interpretation of measurements done by the JUICE mission to constrain critical parameters that can only be observed indirectly: core and shell geometry, their densities, existence and thickness of an internal ocean, to name a few.

✉ Matteo Veglianti
veglianti@mat.uniroma2.it

Christoph Lhotka
lhotka@mat.uniroma2.it

Giuseppe Pucacco
pucacco@roma2.infn.it

[1] University of Rome Tor Vergata, Rome, Italy

Keywords Spin-orbit resonance · Core-shell tidal models · Libration of satellites · Sub-surface ocean

1 Introduction

The planetary moons in our solar system are usually found in so-called spin-orbit resonances, which is also true for the moon of our Earth. The Galilean moons play a special role, not only from a historical point of view, but also since the three inner moons, in addition to the spin-orbit resonance, are also found in a $1:2:4$ mean motion orbital resonance with each other. This special orbital configuration is named Laplace resonance (see, e.g., Lari and Saillenfest 2024; Celletti et al. 2021; Lari et al. 2020). It enables the moon system around planet Jupiter to be in a rather stable configuration with sufficiently large eccentricities that enhance dissipation due to the tidal heating caused by strong gravitational torques from Jupiter (Tobie et al. 2025). In addition, the existence of icy surfaces makes these moons a special class of natural satellites that might host interior layers of liquid water (Spohn and Schubert 2003; Šachl et al. 2025; Kaweeyanun and Masters 2025; De Marchi et al. 2022). The presence of subsurface oceans leads to tidal deformations of the moons up to several meters, being estimated to be only at the level of centimeters in the pure rigid case instead (Tobie et al. 2019; William and Schubert 2003). Moreover, the presence of an inner metallic core being surrounded by a silicate mantle and an icy shell, that is separated by a liquid layer, may also cause an induced magnetic field that can be observed by space probes (Kivelson et al. 2002; Kaweeyanun and Masters 2025; Jia et al. 2025). It is thus of great interest to provide further insights into these very interesting celestial bodies, potentially enabling water-based life in the outer region of the solar system. For a recent review about the current state of the art about the Galilean system see, e.g., Roberts et al. (2023) and Van Hoolst et al. (2024). Recently, the European satellite mission JUICE (Jupiter Icy Moons Explorer) has been sent to the Jovian system to probe the interior of the icy moons and will arrive in 2031. The satellite probe hosts several scientific experiments (see, e.g., Van Hoolst et al. 2024) and dynamical simulations might facilitate the interpretation of the measurements. For rotational studies the radio science experiment 3GM (Cappuccio et al. 2025, 2020; De Marchi et al. 2020) and the laser altimeter GALA (Hussmann et al. 2025) are of special interest. It is widely accepted in the scientific community that observations of the rotational state of the icy surface together with the geophysical interpretation of the interior structure will enable us to constrain the interior (Van Hoolst et al. 2008; Baland and Van Hoolst 2010).

Here, a special interest lies in the modelization and interpretation of the longitudinal librations of surfaces of the moons that are due to gravitational interaction with Jupiter and their static equatorial bulge due to the equilibrium figure. Since the orbits of the moons are eccentric their orbital speed varies and their bulges are not always oriented toward Jupiter, which causes a change in the rotation speed of them that can be seen as librations relative to an exact spin-orbit synchronous state, see, e.g., Van Hoolst et al. (2013) and Furi et al. (2011), or, in terms of a simplified model Burton (1963) and Scoppola et al. (2022). Standard mathematical models that describe these librations are usually based on the assumption of rigid moons (see, e.g., Henrard and Schwanen 2004; Lhotka 2013, 2017). These assumptions can be relaxed by including additional perturbations (see, e.g., Ragazzo et al. 2022; Noyelles 2010). While the rigid rotation of the Galilean satellites has already been investigated e.g., in Rambaux and Henrard (2005), Rambaux et al. (2010), the accurate interpretation of future observations requires the implementation of a theory based on core–shell dynamics. Attempts into this

directions have already been made, e.g., in Van Hoolst et al. (2013), Van Hoolst et al. (2020), Baland and Van Hoolst (2010), Van Hoolst et al. (2008), see also their references therein. More recently, alternative dynamical models, based on creep tide theory, have been used (Folonier and Ferraz-Mello 2017; Folonier et al. 2015; Ferraz-Mello 2013) in which the deformability of the different layers can implicitly be taken into account. However, while coupled spin dynamical problems have been used to model the interaction of the different layers (and separated by liquid layers), effects on longer times have been usually neglected, which is valid on short time scales since the dissipative perturbations are small enough. In this work we argue that a concise study of these small effects may also have great implication on the correct understanding of the interior composition of the moons as well. In fact, dissipative effects, i.e., tides and viscous coupling, strongly depend on parameters that are usually linked with the interior of the moons. Including these effects in the study of the moon's librations on different time scales may provide further constraints on its internal physical parameters.
The investigation of small effects is prone to several potential numerical errors, and the pure numerical treatment of dynamical problems with contributions of terms ranging over several orders of magnitude can be challenging. The step size in the numerical solvers needs to be bounded to avoid problems with the step size controller which can lead to inaccuracies, instability, or even divergence from the true solution. On the one hand, if the step size in numerical solvers is too large, important details and smaller events might be missed. On the other hand, if the step size is too small, the computation time can become inefficient and time-consuming. In the worst scenario, numerical errors that are intrinsic to the numerical methods might result in total errors that can be misinterpreted as physical effects. For this reason we provide a detailed analysis of our results confirmed also by analytical arguments to tackle the mid-term effects with great detail. We remark that long-term effects in the spin-orbit problem in the rigid body case have also been investigated in Lhotka (2013), using a symplectic mapping, Sansottera et al. (2014), using rigorous estimates based on normal forms, and Celletti and Lhotka (2014), investigating the basins of attraction of several spin-orbit resonances. We mainly focus our study on the application to the moon Ganymede. However, we remark that most of the results are valid also for the other Galilean moons as well and can easily be adapted to them once new data from the space mission will become available.
A summary of our assumptions that we make in the dynamical description of the orbit, the rotation, and the moon is as follows. Since the orbital period is much smaller than the precession period of the orbital ellipse and much smaller than any other perturbation (moon–moon gravitational interaction, the effect of the sun, see e.g., Lainey et al. (2006)) an inertial frame can be defined with center of mass of the moon and orientation along the direction of semi-major axis (Bills 2005; Lainey et al. 2006). Moreover, we assume a fixed Keplerian orbit of the moon neglecting further gravitational perturbations (the effect of the other moons, and the sun have been investigated, e.g., in Rambaux et al. (2011)). We notice that as the authors show, the long-periodic effect is important to correctly interpret the measurements, while they affect to a much lesser extent the librations due to core–shell interactions. From the rotational point of view, we also neglect obliquity (indeed, according to Baland et al. (2012); Bills (2005), they are small), i.e., they are only contributing as a second-order effect in the equations of motion of the libration, as well as the wobble (Van Hoolst et al. 2008; Peale 2008). As a consequence in our study the inertial, orbital, rotational, and body z-axes are aligned. Since the moon is found very close to exact spin-orbit resonance we also take advantage of several parameters being small and neglect higher-order effects in the derivation of the equations of motion (some details can be found below; we essentially follow the seminal works Van Hoolst et al. (2008), Baland and Van Hoolst (2010)). Moreover, we neglect the

effect of the tidal deformation on the libration, being due to time-dependent polar moment of inertia, being small, as shown in Baland and Van Hoolst (2010). Small periodic equatorial flattening and small misalignments are neglected (Rambaux et al. 2010). Further unmodeled effects are, e.g., friction between shell and ocean interface.

Our assumptions on the internal structure are the following. We assume that Ganymede is composed of a solid core surrounded by a molten mantle, then a liquid ocean and finally an icy crust, all described in terms of triaxial ellipsoids. Following the idea in Baland et al. (2012), Coyette et al. (2016) and Baland et al. (2019) it is possible to reduce this structure to two dynamical layers that we call *interior* and *exterior*. These two layers are interacting via a conservative gravitational torque proportional to their angular nonalignment. Moreover, a second interaction, proportional to their relative angular velocity, is also present. This viscous interaction is a first source of dissipation and it is due to the presence of the fluid interface between interior and exterior (indeed, according to Juno's data, the liquid interface in the case of Ganymede is supposed to be composed of liquid water, see for instance Casajus et al. (2022)). A second source of friction is due to the viscoelastic structure of the moon, in which the tidal deformation is not completely elastic, implying a certain dissipation. Other kind of interactions between core and crust, such as pressure or electromagnetic coupling, are sometimes considered in literature, for an exhaustive discussion see Rochester (1970). For the aim of this paper, we neglect all this kind of couplings that we implicitly suppose much smaller than the two we are considering. In order to describe the two sources of dissipation in the system we assume a simple viscous friction, linearly dependent on the difference of velocity, for the interaction between interior and exterior, i.e., similar to equation (10) in Correia and Laskar (2009) or equation (53) of Folonier and Ferraz-Mello (2017). Finally, for an overview on tidal dissipation see, e.g., Murray and Dermott (1999), more details can also be found in Efroimsky and Makarov (2013), Efroimsky (2015), Ferraz-Mello et al. (2015).

In our work we essentially follow the mathematical model developed in Peale (2005). To include the elastic response of the different layers due to the tidal deformations we follow the derivations given in (Folonier and Ferraz-Mello 2017; Folonier et al. 2015; Ferraz-Mello 2013).

2 Mathematical framework

A standard derivation of the equation of motion based on a Newtonian approach is shown in Baland et al. (2019). An alternative derivation based on a Lagrangian approach is shown in Pinzari et al. (2024). We follow here the first approach, first deriving the equation for a single layer body and then generalizing the result in order to consider a multilayer body. Variations of the model derived in this section can be found in the next section, including a model based on creep tide theory.

In the noninertial body frame (BF) that rotates with respect to the inertial frame with angular velocity $\mathbf{\Omega}$, the angular momentum equation is:

$$\dot{\mathbf{H}} + \mathbf{\Omega} \times \mathbf{H} = \mathbf{\Gamma}, \tag{1}$$

$\mathbf{H} = I\,\mathbf{\Omega}$ represents the angular momentum, $\dot{\mathbf{H}}$ is its time derivative, I represents the inertia tensor and $\mathbf{\Omega}$ is the rotation vector:

$$\mathbf{\Omega} = \omega_x \mathbf{u_x} + \omega_y \mathbf{u_y} + \omega_z \mathbf{u_z} = \begin{pmatrix} \omega_x \\ \omega_y \\ \omega_z \end{pmatrix}. \tag{2}$$

Here, the polar motion of the rotation axis is described by vector (ω_x, ω_y), and assuming a 1 : 1 spin-orbit resonance, the spin ω_z is given by:

$$\omega_z = n + \dot{\gamma}, \tag{3}$$

where n is the mean motion of the body and γ is the small libration angle. For the purpose of this paper, we assume $\omega_x << n$, $\omega_y << n$ and $\dot{\gamma} << n$. Let $A < B < C$ on the diagonal of I and assume zero off-diagonal terms, up to the first order in polar motion, the left-hand side of equation (1) becomes:

$$\dot{\mathbf{H}} + \boldsymbol{\Omega} \times \mathbf{H} = \begin{pmatrix} A\dot{\omega}_x + (C - B)n\omega_y \\ B\dot{\omega}_y + (A - C)n\omega_x \\ C\ddot{\gamma} \end{pmatrix}. \tag{4}$$

The third component is obtained by replacing ω_z with $n + \dot{\gamma}$ and, since n is constant, considering only the time derivative of $\dot{\gamma}$.
In equation (1) symbol $\boldsymbol{\Gamma}$ represents the general torque on the system in the body frame, composed by: a gravitational torque $\boldsymbol{\Gamma}_\mathbf{g}$ due to a parent body, a viscous torque $\boldsymbol{\Gamma}_\mathbf{v}$ due to the presence of an internal ocean, an inner-gravitational torque $\boldsymbol{\Gamma}_\mathbf{i}$ between two layers, a tidal torque $\boldsymbol{\Gamma}_\mathbf{t}$ with an external body. The gravitational torque is given by $\boldsymbol{\Gamma}_\mathbf{g} = \mathbf{F} \times \mathbf{r}$, with the location of the center of the moon given by $\mathbf{r} = (x, y, z)$ and $\mathbf{F} = -\nabla V$, where the potential V is given by:

$$V = -\sum \frac{GM\delta m}{\Delta} = -GM \sum \frac{\delta m}{(r^2 + R^2 - 2rR\cos\theta)^{\frac{1}{2}}}. \tag{5}$$

Here, G, M are the gravity constant and mass of the planet, respectively. The remaining quantities are the mass element δm with body-centric coordinates (R, θ), with angle θ taken from the direction to and distance Δ from the planet (see e.g., Fig.5.5 in Murray and Dermott 1999). Expanding in powers of $\frac{R}{r} << 1$ and expressing in terms of principal moments of inertia, we obtain:

$$V = -\frac{GMm_T}{r} - \frac{GM}{2r^5}[x^2(B + C - 2A) + y^2(A + C - 2B) + z^2(A + B - 2C)], \tag{6}$$

where m_T is the total mass of the moon. Using the Kepler's third law: $GM = n^2a^3$, with a semimajor axis, we get:

$$\boldsymbol{\Gamma}_\mathbf{g} = 3n^2\left(\frac{a}{r}\right)^3 \begin{pmatrix} (C - B)r_Y r_Z \\ (A - C)r_X r_Z \\ (B - A)r_X r_Y \end{pmatrix}, \tag{7}$$

where $\mathbf{r_{BF}} = (r_X, r_Y, r_Z) = \left(\frac{x}{r}, \frac{y}{r}, \frac{z}{r}\right)$ represents the unit vector in the direction from the mass center of the primary to the position of the secondary. Equation (7) corresponds to equation (5) in Coyette et al. (2016). To express this torque in the body frame, let us choose the first axis of the orbital reference frame into the direction of the secondary: $\mathbf{r_{orb}} = (1, 0, 0)$, see Fig.1. Referenced to the same figure, we perform a rotation from the orbital frame to an inertial nonrotating frame. The x and z axis of the inertial frame point toward the ascending node of the mean orbital plane and toward the axis perpendicular to the mean orbital plane, respectively. In order to do that, we perform a rotation around the z axis by an angle $(-\omega - f + \pi)$;[1] a rotation around the x axis by an angle $(-i)$;[2] and a rotation around the

[1] ω represents the argument of periapsis, f the true anomaly and π arise from the fact that $\mathbf{r}$ is defined from the moon to the planet, that is in the opposite direction with respect to the usual way.

[2] i represents the inclination of the orbital plane with respect to the inertial one

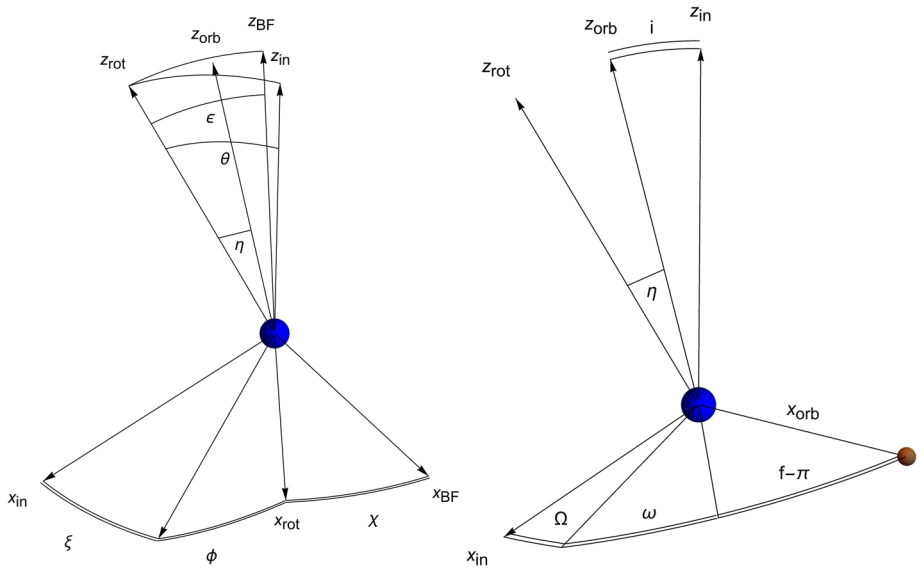

Fig. 1 Rotational (left) and orbital (right) reference frames. See text

z axis by an angle $(-\Omega)$[3]: $\mathbf{r_{in}} = \mathcal{R}_z(-\Omega)\mathcal{R}_x(-i)\mathcal{R}_z(-\omega - f + \pi)(1, 0, 0)$. Next, we perform a transformation to a rotation frame with the z axis along the rotation axis of the primary and the x axis along the ascending node of the plane perpendicular to the rotation axis over the inertial frame: $\mathbf{r_{rot}} = \mathcal{R}_x(\theta)\mathcal{R}_z(\xi)\mathbf{r_{in}}$, where ξ is the longitude of the ascending node of the rotation plane over the inertial one and θ is the inclination of the rotation plane with respect to the inertial one. Finally, the components of $\mathbf{r_{BF}}$ are: $\mathbf{r_{BF}} = \mathcal{R}_z(\chi)\mathcal{R}_x(-\epsilon)\mathcal{R}_z(\phi)\mathbf{r_{rot}}$, where ϕ is the angle between the ascending node of the orbital plane over the inertial plane and the ascending node of the BF plane and the rotation one; ϵ is the inclination of the BF plane with respect to the rotation one; χ is the angle between the ascending node of BF plane over the rotation one and the body frame's x axis. We assume $\alpha \in \{i, \theta, \epsilon\}$ being small. Then replacing $\cos\alpha$ with 1 and $\sin\alpha$ with α and neglecting nonlinear terms, we obtain:

$$\mathbf{r_{BF}} = \begin{pmatrix} \cos(f - \xi - \phi - \chi + \omega + \Omega - \pi) \\ \sin(f - \xi - \phi - \chi + \omega + \Omega - \pi) \\ i\sin(f + \omega - \pi) - \theta\sin(f - \xi + \omega + \Omega - \pi) + \epsilon\cos(f - \xi - \phi + \omega + \Omega - \pi) \end{pmatrix}, \tag{8}$$

that is equation (11) in Coyette et al. (2016). Taking $\xi = \Omega + \sigma$, $\theta = \eta + i$, $f = M + s$, with true and mean anomaly f and M, $s = 2e\sin M + o(e^2)$, with eccentricity e, imposing the synchronous rotation, and performing small angles approximation for all angles $\alpha \in \{i, \theta, \epsilon, \sigma, \eta, s, \gamma\}$, we get:

$$\mathbf{r_{BF}} = \begin{pmatrix} 1 \\ s - \gamma \\ \epsilon\sin(\chi) + \eta\sin(\omega + M) \end{pmatrix}, \tag{9}$$

where

$$\gamma = (\chi + \phi + \xi) - (M + \Omega + \omega - \pi) \tag{10}$$

[3] Ω represents the longitude of the ascending node.

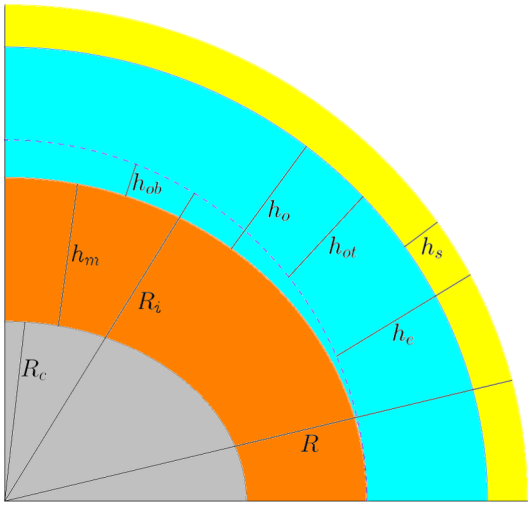

Fig. 2 Internal structure of Ganymede. The layers are not to scale. The core (in gray), the mantle (in orange) and the bottom part of the ocean compose the *interior* part. Top part of the ocean and the crust (in yellow) compose the *exterior* part. The ideal dotted line separates the interior part from the exterior

is the same resonant angle defined in (3). Indeed $(\chi + \phi + \xi)$ is the angle between the axis of the inertial frame x_{in} and the axis of the body frame x_{BF}, that is the direction of the largest axis of symmetry of the body, while $(M + \Omega + \omega - \pi)$ is the position of the central planet in the orbital frame. In order to clarify the geometry, we can consider the special case in which $\eta = \epsilon = i = 0$ (planar problem) and $\Omega + \omega = 0$. In this case the geometry is that represented in Fig. 1 of Celletti and Lhotka (2014): $(\chi + \phi + \xi)$, the angle between x_{in} and x_{BF} is simply x. On the other hand, $(M + \Omega + \omega - \pi)$ becomes, in that case, simply M. Therefore the resonant condition (10) becomes: $\gamma = x - M$. Using (9), expanding r up to the first order in the eccentricity: $r = a(1 - e \sin M)$ and performing again the small angles approximations the torque in (1) becomes:

$$\mathbf{\Gamma_g} = \begin{pmatrix} 0 \\ 3n^2(A - C)[\epsilon \sin(\chi) + \eta \sin(\omega + M)] \\ 3n^2(B - A)(s - \gamma) \end{pmatrix}. \tag{11}$$

Since we are interested in the evolution of the resonant angle γ, we focus from now on only on the third component; then, from (4) and (11) we obtain the following equation for a single layer:

$$C\ddot{\gamma} = \frac{3}{2}n^2(B - A)[4e \sin M - \sin(2\gamma)] + \Gamma_z \tag{12}$$

where we have replaced s with $2e \sin M$ and we have relaxed the small angle approximation, replacing 2γ with $\sin(2\gamma)$. It is equation (5.58) in Murray and Dermott (1999) up to first order in small quantities, with Γ_z representing the third component of other torques beyond that we have just considered.

A generalization to the case of a multilayer body is done as follows. We assume a four-layer structure of the satellite: an inner solid rocky heavy core surrounded by a layer of molten rock, the mantle, then a liquid ocean and finally an external solid thin and light crust, all described in terms of triaxial ellipsoids. Following the idea in Baland et al. (2012), Coyette et al. (2016) and Baland et al. (2019), the ocean is divided into an inner part attached to the mantle and an outer part attached to the crust, the boundary between the two being a sphere with radius equal to the radius of the core+mantle, see Fig.2. Then we call *interior* the internal part of the body, composed of the core and the mantle together with the inner

part of the ocean and *exterior* the external part of the body, composed of the outer part of the ocean together with the crust. Let subscripts i, e and s be used to label the quantities related to the interior, exterior and shell, respectively. In particular, C_i, C_e and C_s are the moments of inertia with respect to the spin direction. The equatorial ellipticities are then given by $\varepsilon_i = \frac{B_i - A_i}{C_i}$ and $\varepsilon_e = \frac{B_e - A_e}{C_s}$ (the presence of C_s in the denominator reflects that the inertia contribution of the exterior arises only from the shell, see Baland et al. (2019)). Hence, we obtain an equation of motion of the form (12), one for each resonant angle γ_i and γ_e, defined using the relation (10). The two equations are coupled by gravitational interaction and the viscous torque due to the internal ocean. Moreover, each layer will experience tidal torques due to Jupiter. The coupled dynamical system describing the multilayer problem is of the form (based on the assumption of rigid double layers, RDL in short hereafter):

$$\begin{cases} \ddot{\gamma}_i = \frac{3}{2} n^2 \varepsilon_i [4e \sin(nt) - \sin(2\gamma_i)] - \frac{k_g}{2C_i} \sin(2\gamma_i - 2\gamma_e) - \frac{\lambda_v}{C_i}(\dot{\gamma}_i - \dot{\gamma}_e) - \frac{\lambda_{ti}}{C_i}(\dot{\gamma}_i - 6ne^2) \\ \ddot{\gamma}_e = \frac{3}{2} n^2 \varepsilon_e [4e \sin(nt) - \sin(2\gamma_e)] - \frac{k_g}{2C_s} \sin(2\gamma_e - 2\gamma_i) - \frac{\lambda_v}{C_s}(\dot{\gamma}_e - \dot{\gamma}_i) - \frac{\lambda_{te}}{C_s}(\dot{\gamma}_e - 6ne^2). \end{cases} \tag{13}$$

The first terms on the right-hand side refer to the single-layer case. The next terms define the gravitational interaction between interior and exterior layers that are proportional to their angular non-alignment. The third terms model the viscous interaction between the two different layers, depending on their relative rotation with different angular velocities. We remark that this form is consistent with the assumption of a laminar regime for the liquid ocean. Finally, the remaining terms correspond to the tidal torque, expanded up to the second order in eccentricity. We notice that we also studied the RDL model based on the unaveraged form of the tidal torques with minor effects on the long-term dynamics. When not explicitely specified the RDL model will refer to the one with the averaged tidal torques, i.e., the above equation. The expressions of the coefficients that enter in equation (13) are the following. For the gravitational interaction:

$$k_g = \frac{8}{5} \pi G (B_i - A_i)[\rho_s(\beta_s - \beta_o) + \rho_o \beta_o)], \tag{14}$$

where ρ_s and ρ_o are the densities of the shell and ocean, respectively, β_s and β_o are their equatorial flattenings, given by $\frac{a-b}{a}$, where a and b are the axes that define the ellipsoidal layer perpendicular to the spin direction. For the viscous interaction we use:

$$\lambda_v = \frac{8}{3} \pi \eta_o \frac{R_i^4}{h_o}, \tag{15}$$

where η_o is the viscosity of the ocean, h_o is its thickness and R_i is the mean radius of the interior layer. For the tidal coefficients we have:

$$\lambda_{ti} = 3 \frac{GM^2}{na^6} \frac{f_i k_{2i}}{Q_i} R_i^5 \quad \text{and} \quad \lambda_{te} = 3 \frac{GM^2}{na^6} \frac{f_e k_{2e}}{Q_e} R_e^5, \tag{16}$$

where M is the mass of Jupiter, R_i and R_e are the radii of the interior and exterior layers, Q_i and Q_e are their tidal quality factors, k_{2i} and k_{2e} are the Love numbers and f_i, f_e are dimensionless factors (see also appendix B, (66)).

There are several parameters entering (13), provided in Table 2, that can be obtained as follows. We start with the parameters published in the recent literature as shown in Table 1. They are related to those of Table 2 as follows (see second column and the geometrical relations shown in Fig. 2). To obtain the moments of inertia of the shell C_s we proceed

Table 1 Physical parameters taken from literature

Parameter	Value	Reference
Jupiter's mass (M)	$1.898 \times 10^{27}\, kg$	N.F.S
Ganymede's total mass (m_T)	$1.482 \times 10^{23}\, kg$	N.F.S
Mean motion (n)	$1.0 \times 10^{-5}\, Hz$	N.F.S
Orbital semimajor axis (a_{orb})	$1.1 \times 10^{9}\, m$	N.F.S
Eccentricity (e)	1.3×10^{-3}	N.F.S
Mean radius (R)	$2631200\, m$	Hay 2019
Core radius (R_c)	$300000\, m$	Sohl 2002
Shell thickness (h_s)	$150000\, m$	N.F.S
Ocean thickness (h_o)	$100000\, m$	N.F.S
Body semimajor axis (a)	$2634570\, m$	Zubarev 2015
Body semimajor axis (b)	$2632970\, m$	Zubarev 2015
Body semimajor axis (c)	$2631380\, m$	Zubarev 2015
Shell density (ρ_s)	$920\, kg/m^3$	DeMarchi 2022
Ocean density (ρ_o)	$1100\, kg/m^3$	DeMarchi 2022
Mantle density (ρ_m)	$3222\, kg/m^3$	Kamata 2016
Core density (ρ_c)	$5330\, kg/m^3$	Kamata 2016
Ocean viscosity (η_o)	$1.57 \times 10^{-3}\, Pa \cdot s$	IAPWS 2008
Interior Love number (k_{2i})	$0.7 \ldots 0.9$	Davies 1998
Exterior Love number (k_{2e})	$0.7 \ldots 0.9$	Davies 1998
Interior quality factor (Q_i)	100	assumed
Exterior quality factor (Q_e)	100	assumed

Table 2 Reference values for the parameters entering (13) constrained by total mass, total volume and mean density of Ganymede

Parameter	Formula	Value
Mean motion (n)	given	$1.00 \times 10^{-5}\, Hz$
Eccentricity (e)	given	1.30×10^{-3}
Shell moment of inertia (C_s)	see text	$4.85 \times 10^{34}\, kg \cdot m^2$
Interior moment of inertia (C_i)	$C_i = \frac{1}{5}(a_i^2 + b_i^2)m_i$	$2.96 \times 10^{35}\, kg \cdot m^2$
Modified interior ellipticity (ε_i)	$\varepsilon_i = \frac{B_i - A_i}{C_i}$	6.07×10^{-4}
Modified shell-exterior ellipticity (ε_e)	$\varepsilon_e = \frac{B_e - A_e}{C_s}$	8.19×10^{-4}
Gravitational coupling factor (k_g)	$k_g = \frac{8}{5}\pi G(B_i - A_i)[\rho_s (\beta_s - \beta_o) + \rho_o \beta_o)]$	$3.67 \times 10^{22}\, kg \cdot m^2/s^2$
Viscous friction coefficient (λ_v)	$\lambda_v = \frac{8}{3}\pi \eta_o \frac{R_i^4}{h_o}$	$4.23 \times 10^{18}\, kg \cdot m^2/s$
Interior tidal coefficient (λ_{ti})	$\lambda_{ti} = 3\frac{GM^2}{na^6}\frac{f_i k_{2i}}{Q_i} R_i^5$	$1.29 \times 10^{25}\, kg \cdot m^2/s$
Exterior tidal coefficient (λ_{te})	$\lambda_{te} = 3\frac{GM^2}{na^6}\frac{f_e k_{2e}}{Q_e} R_e^5$	$1.79 \times 10^{26}\, kg \cdot m^2/s$

numerically. Let W_s be the volume of the shell defined as the region:

$$W_s = \left\{ (x, y, z) \in \mathbb{R}^3 : \frac{x^2}{a^2} + \frac{y^2}{b^2} + \frac{z^2}{c^2} \leq 1, \frac{x^2}{a_o^2} + \frac{y^2}{b_o^2} + \frac{z^2}{c_o^2} \geq 1 \right\}, \tag{17}$$

where a, b, c are the semimajor axes of the full body (see Table 1), and a_o, b_o, c_o refer to the semimajor axes of the ellipsoid that circumscribes the ocean. In principle, they are free parameters; however, due to the lack of knowledge of the actual internal structure, we assume $a_o = a - h_s, b_o = b - h_s, c_o = c - h_s$, with h_s given in Table 1. A more physically consistent approach would be to estimate the static equilibrium flattenings using the theory of figures (see also Sect. 3.3). Then, assuming a constant value for the density of the shell ρ_s (given again in Table 1), the moments of inertia are computed by solving the following integral extended over all the region W_s:

$$I_s = \rho_s \int_{(x,y,z)\in W_s} \begin{pmatrix} y^2+z^2 & -xy & -xz \\ -xy & x^2+z^2 & -yz \\ -xz & -yz & x^2+y^2 \end{pmatrix} dxdydz, \tag{18}$$

and by taking $(A_s, B_s, C_s) = diag(I_s)$. The integrals have numerically been solved using the Wolfram language function MomentsOfInertia. To calculate the polar moment of inertia of interior C_i we need the mass of the interior m_i and the semimajor axes a_i, b_i which are unknown. Therefore we assume a_i/a, b_i/b, c_i/c to be equal $(R - h_{ot} - h_s)/R$, with Ganymede's mean radius R and $h_{ot} = h_o - h_{ob}$ (see Fig. 2). The mass of the interior is determined by $m_i = \rho_i V_i$ with the interior mean density given by the formula $\rho_i = (\rho_c V_c + \rho_m V_m + \rho_o V_{ob})/(V_c + V_m + V_{ob})$. Here, the densities ρ_c, ρ_m and ρ_o are provided in Table 1. The volume of the core is approximated to be spherical, $V_c = 4/3\pi R_c^3$ with R_c given in Table 1. The volume of the mantle is based on the approximation of a spherical shell $V_m = 4/3\pi(R_{cm}^3 - R_c^3)$. Here, its external radius is given by the formula $R_{cm} = R_c + h_m$, with $h_m = R - R_c - h_s - h_o$, where h_o is the ocean thickness, given in Table 1. The volume of the bottom part of the ocean is assumed to be again a spherical shell $V_{ob} = 4/3\pi(R_i^3 - R_{cm}^3)$, with the radius of the interior $R_i = R_c + h_m + h_{ob}$. Here, h_{ob} is the thickness of the bottom part of the ocean (see Fig. 2) that we set to zero for simplicity. Finally, the volume of the interior is calculated on the formula $V_i = 4/3\pi R_i^3$. To compute the equatorial ellipticity of the interior ε_i, we need the moments of inertia of the interior that we determine analytically: $A_i = 1/5(b_i^2 + c_i^2)m_i$, $B_i = 1/5(a_i^2 + c_i^2)m_i$. On the contrary, the equatorial ellipticity of the exterior ε_e requires the moments of inertia of the exterior A_e and B_e that are determined numerically repeating the calculation used to compute C_s. In particular we have to replace a_o, b_o, c_o in (17) with a_i, b_i, c_i. We proceed in the same way assuming $a_i = a - h_e$, $b_i = b - h_e$, $c_i = c - h_e$ (see Fig. 2) and using W_e, I_e to get A_e, B_e, C_e. Notice the two different assumptions to calculate $a_i = (R_i/R)a$ and $a_i = a - h_e$ that have been used to simplify the numerical computations. In the computation of k_g, G is the gravitational constant; β_s and β_o have already been defined after (14). We remark, since we assume $a_s/a = b_s/b = c_s/c$ and $a_o/a = b_o/b = c_o/c$ we have $\beta_s = \beta_o$. Even if this is not true in general (given the differences in density, thickness and response to external potentials), we checked consistency for Ganymede's parameters by comparing with the findings obtained with an alternative model that is implicitly based on the theory of figures (see Sect. 3.3). Most of the quantities entering $\lambda_v, \lambda_{ti}, \lambda_{te}$ have already been discussed above. Ocean viscosity η_o, tidal love numbers k_2 and tidal quality factors Q are given in Table 1. Since the rheological properties of Ganymede are unknown, we use $k_{2i} = 0.7$ and $k_{2e} = 0.9$ to take into account a difference between interior and exterior. The values of Q_i and Q_e are assumed to be equal and the same as Europa. The dimensionless factors $f_i = (\rho_i - \rho_e)/\rho_i$

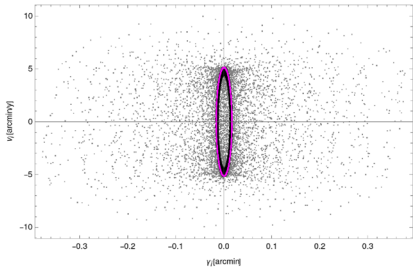

(a) Phase portrait (γ_i, v_i).

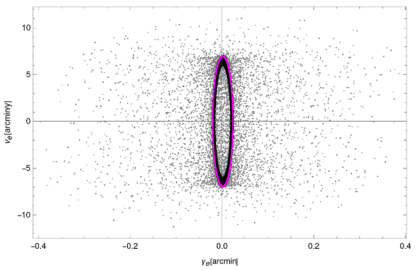

(b) Phase portrait (γ_e, v_e).

Fig. 3 Numerical solution based on RDL (gray/black) and the attractor obtained by VTDL model (magenta)

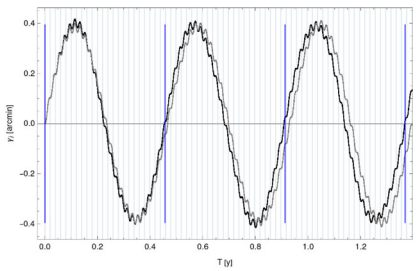

(a) Short term evolution of γ_i for reference values of parameters (in black) and for a smaller value of k_g (in gray).

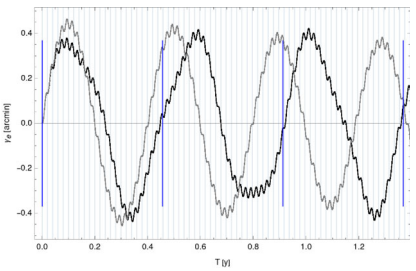

(b) Short term evolution of γ_e for reference values of parameters (in black) and for a smaller value of k_g (in gray).

Fig. 4 Undamped dynamics

and $f_e = R_e^3/[R_e^3 - (R_e - h_e)^3]$ entering the equations (16) are discussed in appendix B. In the next step, we optimize all these values under the constraint to reproduce the total mass, total volume and the mean density of Ganymede. Since most of the quantities are not given with very high accuracy, we use rounded values whenever possible: $\rho_s = 900\,kg/m^3$, $\rho_o = 1000\,kg/m^3$, $\rho_m = 2300\,kg/m^3$ and $\rho_c = 5500\,kg/m^3$. We remark that the variation of the densities is in agreement with values given in Jara-Orué and Vermeersen (2016). With these we recover volume, mass and density published in N.F.S. with less than 1% of inaccuracy. Finally, to have better control on the numerical calculations, we express all quantities in the following unit system: time in sidereal years, masses in Jupiter mass and lengths in Jupiter equatorial radius (YMR units). The values are $e = 0.0013$, $n = 315.58$, $C_s = 5.00\times10^{-9}, C_i = 3.06\times10^{-8}, \varepsilon_i = 6.07\times10^{-4}, \varepsilon_e = 8.19\times10^{-4}, k_g = 3.77\times10^{-6}$, $\lambda_v = 1.38 \times 10^{-17}$, $\lambda_{ti} = 4.21 \times 10^{-11}$, $\lambda_{te} = 5.81 \times 10^{-10}$. We remark that all these parameters can be updated once data from the JUICE mission will be available.

In Fig. 3 we show the projections of the phase space for γ_i (Fig. 3a) and γ_e (Fig. 3b) for the reference values of the Ganymede's parameters. As we can see, after a transient time (gray dots), both variables reach a limit cycle around the origin, corresponding to the black dots. The magenta curve is the attractor that is found analytically from the VTDL model (see section below). The numerical solution based on RDL reaches the analytical attractor. The undamped dynamics is shown in Fig. 4; the damped phase is given in Fig. 8 and will be analyzed, together with the transient time dynamics, in the subsequent sections.

In Fig. 4 we show the short-term evolution of γ_i and γ_e, in the undamped phase, for reference parameters (in black) and for smaller values of k_g (1/100 of the reference value) (in gray). In each signal we can notice the presence of a main sinusoidal term and the presence of a smaller

sinusoidal term. The period of the main term corresponding to the reference parameters is shown by the vertical blue lines, obtained from the imaginary part of the eigenvalues of the VTDL model (see section below), while the period of the smaller term is shown by the light gray vertical lines: it corresponds to the sinusoidal forcing term of frequency n in the equations of motion (13). As we can see from Fig. 4a, the main period of the interior is almost the same for these two choices of the parameters. On the contrary, Fig. 4b shows that the main period of the exterior is subject to change for different parameters. Indeed, comparing the black signals of the two panels, we can see that for the reference value of k_g, the variable γ_e is less regular, but it shows the same period of the interior, as if they behave like a single body. On the contrary, comparing the gray signals, we see that for weak gravitational coupling the periods of interior and exterior are different: they evolve similar to perturbed single layers.

3 Detailed analysis of motion

We perform a detailed analysis of the RDL model (13) and also compare it with a model (EDL), see (53), using a different implementation of the tidal interactions, based on creep tides theory. We investigate the different torques by means of analytical solutions, depending on the physical parameters, of the linearized equations of motion. We provide proper frequencies and estimates on damping time scales, obtained from the real parts of the eigenvalues of the homogeneous solutions. Unless otherwise specified all numerical results are obtained using the reference parameters of Ganymede in the YMR unit system. Our results are validated by direct comparisons with the reference solution. To separate the effect of each torque from the coupling of the layers we are also interested to investigate the effect of the torques on the isolated layers. As a shorthand notation we will use C for conservative, T for tidal, V for viscous models and make use of S and D to distinguish between single- and double-layer cases, e.g., VTDL is used as the abbreviation for the viscous tidal double-layer model.

3.1 Dissipative viscous and tidal effects

The numerical simulations (see Fig. 3) show the contraction of the phase space to a limit cycle in 4 dimensions, which we provide and analyze in the subsequent paragraphs.

VTDL model

For the analytical study we expand (13) up to first order in the small angles γ_e, γ_i to obtain:

$$\begin{cases} \ddot{\gamma}_i = 3n^2\varepsilon_i(2e\sin(nt) - \gamma_i) - \frac{k_g}{C_i}(\gamma_i - \gamma_e) - \frac{\lambda_v}{C_i}(\dot{\gamma}_i - \dot{\gamma}_e) - \frac{\lambda_{ti}}{C_i}(\dot{\gamma}_i - 6ne^2) \\ \ddot{\gamma}_e = 3n^2\varepsilon_e(2e\sin(nt) - \gamma_e) - \frac{k_g}{C_s}(\gamma_e - \gamma_i) - \frac{\lambda_v}{C_s}(\dot{\gamma}_e - \dot{\gamma}_i) - \frac{\lambda_{te}}{C_s}(\dot{\gamma}_e - 6ne^2). \end{cases} \tag{19}$$

These equations correspond to a couple of damped and forced harmonic oscillators with proper frequencies given by:

$$\omega_{0i} = \sqrt{3n^2\varepsilon_i + \frac{k_g}{C_i}} \quad \text{and} \quad \omega_{0e} = \sqrt{3n^2\varepsilon_e + \frac{k_g}{C_s}}. \tag{20}$$

Their rounded values are:

$$\omega_{0i} = 17.46, \quad \text{and} \quad \omega_{0e} = 31.59. \tag{21}$$

Let $v_i = \dot{\gamma}_i$, $v_e = \dot{\gamma}_e$ to write (19) into the form:

$$\dot{\vec{x}} = A\vec{x} + \vec{b}, \tag{22}$$

with: $\vec{x} = (\gamma_i, v_i, \gamma_e, v_e)$, $\vec{b} = \left(0, 6n^2\varepsilon_i e \sin(nt) + \frac{6ne^2\lambda_{ti}}{C_i}, 0, 6n^2\varepsilon_e e \sin(nt) + \frac{6ne^2\lambda_{te}}{C_s}\right)$ and

$$A = \begin{pmatrix} 0 & 1 & 0 & 0 \\ -\omega_{0i}^2 & -\frac{\lambda_{ti}+\lambda_v}{C_i} & \frac{ki}{C_i} & \frac{\lambda_v}{C_i} \\ 0 & 0 & 0 & 1 \\ \frac{ki}{C_s} & \frac{\lambda_v}{C_s} & -\omega_{0e}^2 & -\frac{\lambda_{te}+\lambda_v}{C_s} \end{pmatrix}. \tag{23}$$

The homogeneous solution of (22) requires to solve for the eigensystem of A. The eigenvalues are obtained from the characteristic polynomial:

$$\begin{aligned} x^4 + \left(\frac{\lambda_{te}+\lambda_v}{C_s} + \frac{\lambda_{ti}+\lambda_v}{C_i}\right)x^3 + \left(\omega_{0i}^2 + \omega_{0e}^2 + \frac{\lambda_{ti}\lambda_{te}}{C_iC_e} + \frac{\lambda_{ti}\lambda_v}{C_iC_e} + \frac{\lambda_{te}\lambda_v}{C_iC_e}\right)x^2 \\ + \left(\frac{\lambda_v\omega_{0i}^2}{C_s} + \frac{\lambda_v\omega_{0e}^2}{C_i} - \frac{2\lambda_v k_g}{C_sC_i} + \frac{\lambda_{te}\omega_{0i}^2}{C_s} + \frac{\lambda_{ti}\omega_{0e}^2}{C_i}\right)x + \omega_{0i}^2\omega_{0e}^2 - \frac{k_g}{C_iC_s} = 0. \end{aligned} \tag{24}$$

Their values are (we use j for the imaginary unit):

$$\begin{aligned} l_{1,2} &= -5.09 \cdot 10^{-2} \pm 33.36\,\mathrm{j} \\ l_{3,4} &= -7.83 \cdot 10^{-3} \pm 13.78\,\mathrm{j} \end{aligned} \tag{25}$$

Explicit expressions for the eigenvalues can be found from (24). Approximate expressions, that keep the dependencies on the parameters, have been derived by setting $\lambda_{ti} = \lambda_{te} = 0$ or $\lambda_v = 0$, respectively (see appendix D). We call the corresponding models that allow to separate the effects of the viscous from the effect of the tidal torques, VDL and TDL, respectively. As it turns out for Ganymede, the eigenvalues of the VTDL model agree with the eigenvalues of the TDL model (up to significant digits) from which we conclude that the damping time scales are dominated by the tides due to Jupiter.
The particular solution for the sinusoidal forcing term is found by the ansatz:

$$\vec{x}_{ps}(t) = \begin{cases} \gamma_{ps,i}(t) = A_i \sin(nt + \alpha_i) = \frac{1}{2}A_i\mathrm{j}e^{-\mathrm{j}nt-\mathrm{j}\alpha_i} - \frac{1}{2}A_i\mathrm{j}e^{\mathrm{j}nt+\mathrm{j}\alpha_i} \\ v_{ps,i}(t) = nA_i \cos(nt + \alpha_i) = \frac{1}{2}nA_i\mathrm{j}e^{-\mathrm{j}nt-\mathrm{j}\alpha_i} + \frac{1}{2}nA_i\mathrm{j}e^{\mathrm{j}nt+\mathrm{j}\alpha_i} \\ \gamma_{ps,e}(t) = A_e \sin(nt + \alpha_e) = \frac{1}{2}A_e\mathrm{j}e^{-\mathrm{j}nt-\mathrm{j}\alpha_e} - \frac{1}{2}A_e\mathrm{j}e^{\mathrm{j}nt+\mathrm{j}\alpha_e} \\ v_{ps,e}(t) = nA_e \cos(nt + \alpha_e) = \frac{1}{2}nA_e\mathrm{j}e^{-\mathrm{j}nt-\mathrm{j}\alpha_e} + \frac{1}{2}nA_e\mathrm{j}e^{\mathrm{j}nt+\mathrm{j}\alpha_e} \end{cases} \tag{26}$$

with free parameters A_i, A_e, α_i, α_e, determined by substitution in (22):

$$A_i = 4.75 \cdot 10^{-6},\ A_e = 6.42 \cdot 10^{-6} \quad \text{and} \quad \alpha_i = \pi, \alpha_e = \pi \tag{27}$$

The constant particular solution is given by:

$$\vec{x}_{pc}(t) = \begin{cases} \gamma_{pc,i}(t) = \frac{6ne^2\lambda_{ti}}{\omega_{0i}^2 C_i} + \frac{6ne^2(k_g^2\lambda_{ti} + k_g\lambda_{te}C_i\omega_{0i}^2)}{\omega_{0i}^2 C_i(C_sC_i\omega_{0i}^2\omega_{0e}^2 - k_g^2)} \\ v_{pc,i}(t) = 0 \\ \gamma_{pc,e}(t) = \frac{6ne^2\lambda_{te}}{\omega_{0e}^2 C_s} + \frac{6ne^2(k_g^2\lambda_{te} + k_g\lambda_{ti}C_s\omega_{0e}^2)}{\omega_{0e}^2 C_s(C_iC_s\omega_{0e}^2\omega_{0i}^2 - k_g^2)} \\ v_{pc,e}(t) = 0 \end{cases} \tag{28}$$

The two nonvanishing solutions $\gamma_{pc,i}$ and $\gamma_{pc,e}$ define the shifts from the origin of the limit cycles shown in Fig. 3; their numerical values are $\gamma_{pc,i} = 2.38 \cdot 10^{-7}$, $\gamma_{pc,e} = 5.52 \cdot 10^{-7}$.

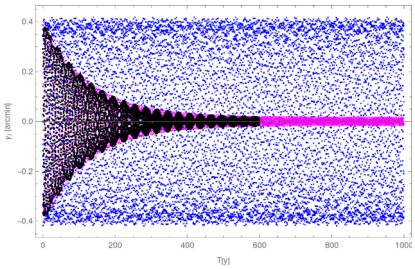

(a) evolution of γ_i for reference values of parameters compared with double layers analytical models.

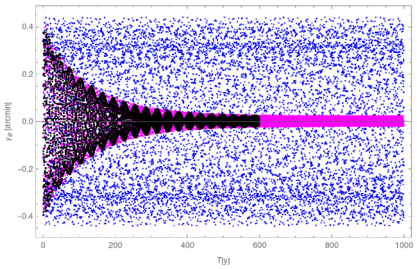

(b) evolution of γ_e for reference values of parameters compared with double layers analytical models.

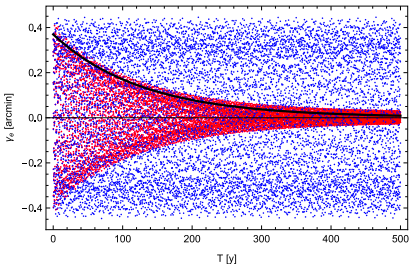

(c) evolution of γ_e for reference values of λ_{ti} and λ_{te}.

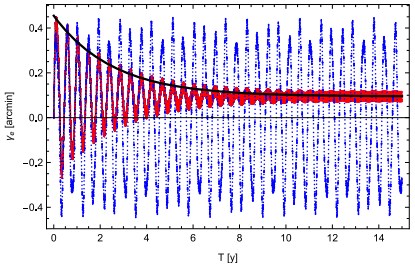

(d) evolution of γ_e for larger values of λ_{ti} and λ_{te}.

Fig. 5 Rotational evolution of γ_i and γ_e for two different choices of the parameters

By linearity, the complete solution of equation (22) is:

$$\vec{x}(t) = \vec{x}_h(t) + \vec{x}_{ps}(t) + \vec{x}_{pc}(t) = c_1 e^{l_1 t}\vec{u}_1 + c_2 e^{l_2 t}\vec{u}_2 + c_3 e^{l_3 t}\vec{u}_3 + c_4 e^{l_4 t}\vec{u}_4 + \vec{x}_{ps}(t) + \vec{x}_{pc}(t). \tag{29}$$

with c_1, c_2, c_3, c_4 depending on initial conditions. The solution (29) has been used to reproduce the orbit shown in magenta in Fig. 3.

In Fig. 5 we can see the evolution of γ_i and γ_e for different values of the parameters. In each figure we compare the analytical solutions obtained with different models: VDL in blue, TDL in red and VTDL in magenta and RDL in black. As we can see, the numerical solution of the RDL model is in perfect agreement with the analytical one (panels a, b).

For reference values of the parameters λ_{ti}, λ_{te} (from Table 2 and of the order of 10^{-10}, 10^{-11} in terms of the YMR units) we see that the damping time scale of the VTDL model is dominated by the tidal one, while the viscous coupling (in blue, VDL model) does not provide sufficient damping strength. We conclude that the ocean alone is not sufficient to damp the system on reasonable time scales, while the damping time scales (linear coefficient in front of time t in the exponential part of the solution) turns out to be dominated by the tidal forces and is of the order of 100 years, as it is shown in panel c. In panel d we show the same dynamics for big values of the tidal coefficients λ_i and λ_e (50 times the reference values). We can see that the damping time scales are now of the order of $3-5$ years (approaching the value obtained in fig. 7a). Moreover, increasing the tidal coefficients, the constant particular solution $\vec{x}_{pc}$ from (28) becomes large enough to be visible as appreciated in the respective figure. Finally, the black line on the bottom of Fig. 5 corresponds to the convex hull obtained from the dominant exponential functions of the VTDL solution for γ_e, equation (29).

VTSL model

In order to study the effect of the ocean, as a perturbation, on an isolated single layer, we define a simplified model starting with (19). Taking $k_g = 0$ and $\dot{\gamma}_i = 0$ (for the study of the outer layer) or $\dot{\gamma}_e = 0$ (for the study of the inner layer), we obtain equations of the form:

$$\ddot{\gamma} + \frac{(\lambda_v + \lambda_t)}{C}\dot{\gamma} + \omega_0^2 \gamma = 6n^2 e\varepsilon \sin nt + \frac{6ne^2\lambda_t}{C}, \tag{30}$$

where we have omitted the subscripts and defined

$$\omega_0 = \sqrt{3n^2\varepsilon}. \tag{31}$$

The solution of the homogeneous equation is:

$$\gamma_h(t) = c_1 e^{\frac{1}{2}t\left(-\frac{(\lambda_v+\lambda_t)}{C} - \frac{\sqrt{(\lambda_v+\lambda_t)^2 - 4C^2\omega_0^2}}{C}\right)} + c_2 e^{\frac{1}{2}t\left(-\frac{(\lambda_v+\lambda_t)}{C} + \frac{\sqrt{(\lambda_v+\lambda_t)^2 - 4C^2\omega_0^2}}{C}\right)}, \tag{32}$$

with $c_1, c_2 \in \mathbb{C}$ depending on the initial conditions ($\gamma(0) = \gamma_0$, $\dot{\gamma}(0) = v_0$). The particular solution of (30) is given by linearity as the sum of two independent forcing terms. The constant part, and related to the shift of the damped solution, is given by:

$$\gamma_{pc}(t) = \frac{6ne^2\lambda_t}{C\omega_0^2}. \tag{33}$$

The solution for the sinusoidal forcing term is found by the ansatz:

$$\gamma_{ps}(t) = A\sin(nt + \alpha) = \frac{1}{2}Aje^{-\mathrm{j}nt - \mathrm{j}\alpha} - \frac{1}{2}Aje^{\mathrm{j}nt + \mathrm{j}\alpha}, \tag{34}$$

with free parameters A, α, determined by substitution in (30):

$$\alpha = \arctan\left(\frac{n(\lambda_v + \lambda_t)}{C(n^2 - \omega_0^2)}\right), \quad A = \frac{6Cn^2\varepsilon e}{\sqrt{C^2(n^2 - \omega_0^2)^2 + n^2(\lambda_v + \lambda_t)^2}}. \tag{35}$$

Then, the complete solution of equation (30) is given by the sum:

$$\begin{aligned}\gamma(t) = \gamma_h(t) + \gamma_{pc}(t) + \gamma_{ps}(t) &= c_1 e^{\frac{1}{2}t\left(-\frac{(\lambda_v+\lambda_t)}{C} - \frac{\sqrt{(\lambda_v+\lambda_t)^2 - 4C^2\omega_0^2}}{C}\right)} \\ &+ c_2 e^{\frac{1}{2}t\left(-\frac{(\lambda_v+\lambda_t)}{C} + \frac{\sqrt{(\lambda_v+\lambda_t)^2 - 4C^2\omega_0^2}}{C}\right)} \\ &+ \frac{6Cn^2\varepsilon e}{\sqrt{C^2(n^2 - \omega_0^2)^2 + n^2(\lambda_v + \lambda_t)^2}} \\ &\times \sin\left[nt + \arctan\left(\frac{n(\lambda_v + \lambda_t)}{C(n^2 - \omega_0^2)}\right)\right] + \frac{6ne^2\lambda_t}{C\omega_0^2}.\end{aligned} \tag{36}$$

An approximate form of c_1, c_2 up to the first order in $e, \varepsilon, \gamma_0, \frac{v_0}{\omega_0}, \frac{\lambda_t}{2C\omega_0}, \frac{\lambda_v+\lambda_t}{2C\omega_0}$ is given by:

$$\begin{cases} c_1 = \frac{\gamma_0}{2} + \mathrm{j}\left(\frac{v_0}{2\omega_0} + \frac{3n^2\varepsilon e}{\omega_0(n^2-\omega_0^2)} + \frac{\gamma_0(\lambda_v+\lambda_t)}{4C\omega_0}\right) \\ c_2 = \frac{\gamma_0}{2} - \mathrm{j}\left(\frac{v_0}{2\omega_0} + \frac{3n^2\varepsilon e}{\omega_0(n^2-\omega_0^2)} + \frac{\gamma_0(\lambda_v+\lambda_t)}{4C\omega_0}\right) \end{cases}. \tag{37}$$

A comparison between approximate and exact values of c_1, c_2 for Ganymede's parameters (Table 1, 2) shows the validity of these expressions up to machine precision. We notice the presence of the term $n^2 - \omega_0^2$ in (37) which implies $\varepsilon \neq 1/3$ for the solution to be valid, which is true for most planetary moons.
We notice that it is possible to focus on the isolated effects due to the viscous torque (VSL model by setting $\lambda_t = 0$) or due to the tidal torque (TSL model by setting $\lambda_v = 0$), analogously to the double-layer case. In this case, the equations of motion, the corresponding solutions and the constants c_1 and c_2 can be derived from equations (30), (36) and (37), setting $\lambda_t = 0$ or $\lambda_v = 0$, respectively. A comparison between (20) and (31) as well as between (28) and (33) shows that we can treat the double layer as a correction of the single layer (see also 4 and 6a).

3.2 Conservative dynamics

In this section we focus on the isolated effect of the conservative gravitational torque due to the parent planet based on the linearized version of (13) and neglecting both the viscous and the tidal contributions. The conservative double-layer model (CDL) is defined by (19) with $\lambda_v = \lambda_{ti} = \lambda_{te} = 0$. The equations of motion are still in the form (22), with:

$$A = \begin{pmatrix} 0 & 1 & 0 & 0 \\ -\omega_{0i}^2 & 0 & \frac{ki}{C_i} & 0 \\ 0 & 0 & 0 & 1 \\ \frac{ki}{C_s} & 0 & -\omega_{0e}^2 & 0 \end{pmatrix}, \quad \vec{b} = \begin{pmatrix} 0 \\ 6n^2\varepsilon_i e \sin(nt) \\ 0 \\ 6n^2\varepsilon_e e \sin(nt) \end{pmatrix} \tag{38}$$

This system corresponds to a couple of forced harmonic oscillators, with proper frequencies given by (20), that are the same for all models, since they share the same internal structure of the moon (and only depend on k_g, ε_i and ε_e). The eigenvalues are obtained from the characteristic polynomial and also compare with (24):

$$x^4 + \left(\omega_{0i}^2 + \omega_{0e}^2\right) x^2 + \omega_{0i}^2\omega_{0e}^2 - \frac{k_g}{C_i C_s} = 0, \tag{39}$$

with the four solutions as follows.

$$\begin{aligned} l_{1,2} &= \pm\frac{\sqrt{-C_i^2C_s^2(\omega_{0e}^2+\omega_{0i}^2) - C_i^{3/2}C_s^{3/2}\sqrt{4k_g^2 + C_sC_i(\omega_{0e}^2-\omega_{0i}^2)^2}}}{\sqrt{2}C_iC_s} \\ l_{3,4} &= \pm\frac{\sqrt{-C_i^2C_s^2(\omega_{0e}^2+\omega_{0i}^2) + C_i^{3/2}C_s^{3/2}\sqrt{4k_g^2 + C_sC_i(\omega_{0e}^2-\omega_{0i}^2)^2}}}{\sqrt{2}C_iC_s} \end{aligned} \tag{40}$$

Their rounded values are:

$$\begin{aligned} l_{1,2} &= \pm 33.36\,\mathrm{j} \\ l_{3,4} &= \pm 13.78\,\mathrm{j} \end{aligned} \tag{41}$$

Comparing (25) and (41) we notice that the imaginary parts of the eigenvalues are in agreement. This means that the frequencies of oscillation of γ_i and γ_e are dominated by the conservative gravitational torque due to Jupiter. The dissipative torques give rise to corrections (not shown here) that are, however, negligible within our approximations. Expanding

(40) up to the first order in the small parameters, we get:

$$l_{1,2} = \pm \mathrm{j}\left(\omega_{0e} + \frac{k_g^2}{2C_sC_i\omega_{0e}(\omega_{0e}^2 - \omega_{0i}^2)}\right)$$
$$l_{3,4} = \pm \mathrm{j}\left(\omega_{0i} - \frac{k_g^2}{2C_sC_i\omega_{0i}(\omega_{0e}^2 - \omega_{0i}^2)}\right). \tag{42}$$

We see that the dominant parts are given by their own proper frequencies ω_{0e}, ω_{0i}. The coupling between the two layers induces correction terms that might explode for $\omega_{0e} \simeq \omega_{0i}$, which is not the case for Ganymede (see (21)). Numerical values of the approximate eigenvalues are:

$$l_{1,2} = \pm 33.71\,\mathrm{j}$$
$$l_{3,4} = \pm 13.62\,\mathrm{j} \tag{43}$$

The relative difference between the values obtained from the approximate expressions and those obtained from expressions (40) turns out to be of the order 10^{-3}, and we confirm that this difference can be decreased by considering higher-order expansions. The particular solution for the sinusoidal forcing term $\vec{x}_{ps}(t)$ can be found by (26) that leads to the following, exact, expressions for the four free parameters A_i, A_e:

$$\begin{cases} A_i = \pm\frac{6n^2eC_s[k_g\varepsilon_e + C_i\varepsilon_i(\omega_e^2 - n^2)]}{k_g^2 - C_iC_s(\omega_i^2 - n^2)(\omega_e^2 - n^2)} \\ A_e = \pm\frac{6n^2eC_i[k_g\varepsilon_i + C_s\varepsilon_e(\omega_i^2 - n^2)]}{k_g^2 - C_iC_s(\omega_i^2 - n^2)(\omega_e^2 - n^2)} \end{cases} \tag{44}$$

Their rounded values are:

$$A_i = 4.75 \cdot 10^{-6},\ A_e = 6.42 \cdot 10^{-6} \tag{45}$$

Comparing (27) and (45), we can see that the amplitudes of the forced solutions still remain the same, while the underlying expressions are different. This means that they are dominated by the conservative torque, i.e., (46), while the effect of the dissipative torques is mainly to reach the forced solution.

The complete solution of equations of motion is given by the sum:

$$\vec{x}(t) = c_1e^{l_1t}\vec{u}_1 + c_2e^{l_2t}\vec{u}_2 + c_3e^{l_3t}\vec{u}_3 + c_4e^{l_4t}\vec{u}_4 + \vec{x}_{ps}(t). \tag{46}$$

where the $\vec{u}_k$ are the eigenvectors of (38) and $\vec{x}_{ps}$ is given by (26) with A_i, A_e given by (44). The four constants c_1, c_2, c_3, c_4 can be obtained from initial conditions ($\gamma_i(0) = \gamma_{0i}$, $\dot{\gamma}_i(0) = v_{0i}$, $\gamma_e(0) = \gamma_{0e}$, $\dot{\gamma}_e(0) = v_{0e}$). Approximate expressions for these constants are given in appendix. Their numerical values depending on initial conditions are:

$$c_{1,2} = 0.45\,v_{0e} - 0.43\,v_{0i} \pm \mathrm{j}\,(15.02\,\gamma_{0e} - 14.32\,\gamma_{0i})$$
$$c_{3,4} = 0.055\,v_{0e} + 0.43\,v_{0i} \pm \mathrm{j}\,(0.74\,\gamma_{0e} + 5.79\,\gamma_{0i})\,. \tag{47}$$

For completeness, we provide the effect of Jupiter on a single perturbed layer only; the dynamical equation (CSL model) is given by:

$$\ddot{\gamma} + \omega_0^2\gamma = 6n^2e\varepsilon\sin nt, \tag{48}$$

with $\omega_0 = \sqrt{3n^2\varepsilon}$. Notice that (48) can be obtained from (30) by setting $\lambda_v = \lambda_t = 0$. Therefore, the solution of (48) is given by (36) and setting $\lambda_v = \lambda_t = 0$:

$$\gamma(t) = \gamma_h(t) + \gamma_p(t) = \frac{1}{2}c_1e^{-\mathrm{j}\omega_0t} + \frac{1}{2}c_1e^{\mathrm{j}\omega_0t} + \frac{1}{2}\mathrm{j}c_2e^{-\mathrm{j}\omega_0t}$$

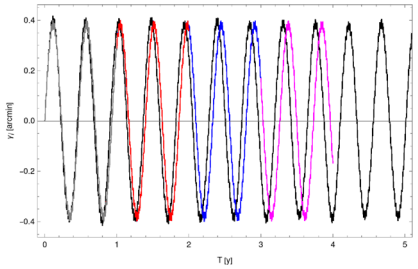

(a) short term evolution of γ_i for reference values of parameters compared with single layer analytical solutions.

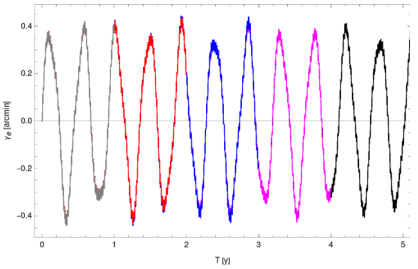

(b) short term evolution of γ_e for reference values of parameters compared with double layers analytical solutions.

Fig. 6 Modular analysis

$$-\frac{1}{2}\mathrm{j}c_2 e^{\mathrm{j}\omega_0 t} - \frac{3en^2\varepsilon}{n^2-\omega_0^2}\mathrm{j}e^{-\mathrm{j}nt} + \frac{3en^2\varepsilon}{n^2-\omega_0^2}\mathrm{j}e^{\mathrm{j}nt}. \tag{49}$$

The two constants c_1 and c_2 depend on initial conditions ($\gamma(0) = \gamma_0$, $\dot{\gamma}(0) = v_0$):

$$\begin{cases} c_1 = \gamma_0 \\ c_2 = \frac{n^2 v_0 - \omega_0^2 v_0 + 6n^3\varepsilon e}{n^2\omega_0 - \omega_0^3} = \frac{v_0}{\omega_0} + \frac{6n^3\varepsilon e}{\omega_0(n^2-\omega_0^2)}. \end{cases} \tag{50}$$

Notice that these expressions are recovered by performing the combinations $c_2 + c_1$ and $\mathrm{j}(c_2 - c_1)$ for c_1 and c_2 given by (37) and setting $\lambda_v = \lambda_t = 0$. In Fig. 6 we can see the short-term evolution of γ_i (panel (a)) γ_e (panel (b)) for reference value of Ganymede's parameters. In each panel we compare the numerical solution (in black) with the analytical ones obtained with different models: conservative model (CSL and CDL) in gray, tidal model (TSL and TDL) in red, viscous model (VSL and VDL) in blue and viscous tidal model (VTSL and VTDL) in magenta. Figure 6a shows that the analytical solutions based on the single-layer model are able to reproduce the numerical signal, suggesting that the coupling due to the exterior acts as a perturbation to the dynamics of the interior layer (with perturbing parameter k_g). On the contrary, from Fig. 6b we can see that the analytical solutions of the double-layer models are in perfect agreement with the numerical signal, showing also that for short-term evolution each analytical model is equally good.

3.3 Elastic tidal response

We also compare our results with an alternative model based on creep tides following (see, e.g., Folonier and Ferraz-Mello 2017; Folonier et al. 2015; Ferraz-Mello 2013). Let σ_k be the distance from the center of gravity to a point on the surface of a triaxial ellipsoid that is assumed to be the equilibrium figure of the k-th elastic layer of the moon, and let ζ_k be the distance of a surface point, along the same radial line as σ_k, on the layer itself. Let the relaxation factor γ_k (not to be confused with γ) be defined by

$$\gamma_k = \frac{(\rho_k - \rho_{k+1})g_k R_k}{2\eta_k}, \tag{51}$$

where g_k is the gravity acceleration on the surface of the k-th layer, and quantities ρ_k, ρ_{k+1}, R_k, η_k are the usual densities, radii and viscosities of the indexed layers. In this framework,

the response of the k-th layer to tidal deformations can be modeled using

$$\dot{\zeta_k} = \gamma_k(\sigma_k - \zeta_k). \tag{52}$$

As it can be shown the units of γ_k are frequencies that formally tend to zero for solid bodies and tend to infinity for fluid ones. Following the exposition in Folonier and Ferraz-Mello (2017) (hereafter PI in short) the basic dynamical model (hereafter EDL in short) for a body composed of two layers is given by (see their equation (54)):

$$\begin{cases} C_c\dot{\Omega}_c = -M_{zc} + \Gamma_c + \Phi_c \\ C_s\dot{\Omega}_s = -M_{zs} + \Gamma_s + \Phi_s. \end{cases} \tag{53}$$

Here, the symbols C_c, C_s are the usual polar moments of inertia (we assume in the following the equivalence between *core* and *interior* and between *shell* and *exterior*), while Ω_c, Ω_s are the spin velocities of the two layers, respectively. The tidal torques M_{zc}, M_{zs}, the gravitational torques Γ_c, Γ_s, as well as the viscous torques Φ_c, Φ_s are provided in equations (44), (50), (52) in PI, respectively. For the aim to compare the RDL and EDL models we relate their different dynamical variables with each other as follows. While in the former, the libration angle γ_k (not to be confused with γ) of the k-th layer is defined in (3), in the latter the spin velocities are related via $\Omega_k = \dot{\hat{\varphi}}_k$ (see, e.g., equation (3) of PI), where the symbol $\hat{\varphi}_k$ represents the angle between the semimajor axis of the $k-$th layer and a given reference direction. Comparing with ω_z in (3), we get the relation between the dynamical variables of the two models: $\Omega_k = n + \dot{\gamma}_k$. In the planar approximation we can choose the argument of periapsis as reference direction, then: $\hat{\varphi}_k = f + \theta_k$, with θ_k being the angle between the position of the planet and the semi-major axis of the k-th layer (see, e.g., Fig.18 in PI). Hence, up to the first order in e: $\gamma_k = \hat{\varphi}_k - M = f + \theta_k - M = 2e \sin M + \theta_k$.
In order to compare the RDL model (13) and the EDL model we rewrite (53) in terms of γ_c, γ_s using this relation to obtain:

$$\begin{cases} \ddot{\gamma}_c = -\frac{M_{zc}}{C_c} - \frac{K}{C_c}\sin\left[2(\gamma_c - \gamma_s)\right] - \frac{\mu}{C_c}(\dot{\gamma}_c - \dot{\gamma}_s) \\ \ddot{\gamma}_s = -\frac{M_{zs}}{C_s} - \frac{K}{C_s}\sin\left[2(\gamma_s - \gamma_c)\right] - \frac{\mu}{C_s}(\dot{\gamma}_s - \dot{\gamma}_c). \end{cases} \tag{54}$$

In this notation the form of the intergravitational torques (2nd terms on the rhs.) and the viscous ones (3rd terms on the rhs.) is the same in both models, compared (54) with (13) (see appendix C for further details). In (54) symbols K, μ are the gravitational coupling constant and friction parameter, respectively, that we can easily relate to constants k_g and λ_v in (13). It remains to discuss the remaining terms in the EDL and RDL models, i.e., the forcing terms (first terms) and averaged tidal torque (last terms) in (13) with the implementation of the tidal torques M_{zc}, M_{zs} in (54). These terms are of particular importance, not only because they are responsible for the long-term dynamics of the system (see, e.g., (26), (28)), but also since they describe the key difference between the EDL and RDL models. We provide as an example, using (15) of PI, and by setting $k = 0$, a term entering the elastic torques:

$$\langle M_{zi}\rangle_0 = \frac{3}{2}n^2 C_i E_{2,0}^2 \bar{\epsilon}_\rho \frac{R_i^5 H_i \sin\sigma_{i,0}\cos\sigma_{i,0} - R_{i-1}^5 H_{i-1}\sin\sigma_{i-1,0}\cos\sigma_{i-1,0}}{R_i^5 - R_{i-i}^5}. \tag{55}$$

Here $E_{2,0}$ is the Cayley coefficient ($E_{2,0} \simeq 1 - \frac{5}{2}e^2$), $\bar{\epsilon}_\rho$ is the flattening of the Jeans spheroid (defined in PI), R_i and R_{i-1} are the mean radii of the exterior and interior surfaces of the i-th layer, H_i and H_{i-1} are the corresponding Clairaut numbers and $\sigma_{i,0}$, $\sigma_{i-1,0}$ are the corresponding phases (see figure 18 of PI). Their values obtained from Table 1, 2 are given in Table 3, 4; their calculation is provided at the end of this section. In the following we just

Table 3 Ganymede's parameters for core and shell entering (53)

Parameter		Core	Shell
Outer radius ($10^6\ m$)	R_k	2.381	2.631
Clairaut number	H_k	0.851	0.865
Axial moment of inertia ($10^{34}\ kg\,m^2$)	C_k	29.50	7.766
Equatorial flattening (tidal) (10^{-4})	ϵ_k	5.603	5.696
Relative height of the elastic tide (10^{-2})	λ_k	6.643	6.643
Relaxation factor ($10^{-8}\ s^{-1}$)	γ_k	6.948	8.662

Table 4 Ganymede's parameters entering (53)

Parameter		value
Ganymede's tidal parameter ($10^{-14}\ s^{-2}$)	τ	9.873
Friction parameter ($10^{18}\ kg\,m^2\,s^{-1}$)	μ	4.228
Gravitational coupling constant ($10^{22}\ kg\,m^2\,s^{-2}$)	K	1.687
Orbital eccentricity	e	0.0013
Orbital mean motion (s^{-1})	n	10^{-5}

aim to summarize some of the aspects that need to be taken into account in the interpretation of the results given in the next section; a full discussion of creep tides is beyond the scope of the current study (for more information see, e.g., Ferraz-Mello 2013; Ferraz-Mello et al. 2015). The damped solution in the RDL model describes a special rotational configuration of the body composed of rigid layers near the synchronous state with an external perturber: the synchronous state is achieved in terms of a special solution of γ_i, γ_e on an attractor (see Fig. 3). In the EDL model the layers keep on deforming toward their equilibrium surface configurations during their orbital evolution. As it has been shown in the previous paragraphs the damping time scales in the RDL model are proportional to the magnitudes of the tidal coefficients $\lambda_{ti}, \lambda_{te}$, while in the EDL model the important time scales to be considered are the damping time scales (or better relaxation time scales) toward their equilibrium figures, (which has been shown to be proportional to γ, see, e.g., Ferraz-Mello et al. 2015). To be more precise, while in the RDL model the damping takes place on static deformed layers—the layers in the EDL model continue to deform with time (no permanent deformation exist in the creep tide model). For this reason a direct comparison of the two models seems to be arbitrary. However, since the parameters that enter (13) and (53) are derived from the same rheological properties of the moon, it is worthwhile to compare the results of the two dynamical systems in the interpretation of experimental data of future space missions.

The outer radius of the core is given by $R_c = R - h_o - h_s$, with mean body radius R, the thickness of the ocean h_o and the thickness of the icy crust h_s, while the radius of the shell $R_s = R$ is the mean radius of Ganymede, where we take h_o, h_s, R from Table 1. The Clairaut numbers of the core (H_c) and the shell (H_s) are obtained on the basis of the four-layer structure (see Fig. 2) as follows. First, we identify $\rho_c, \rho_m, \rho_o, \rho_s$, given in Table 1, with the densities d_k (notation in PI), and R_c, $R_c + h_m$, $R - h_s$, R (notation in Fig. 2) with the radii R_k (notation in PI). Next, we calculate the normalized equatorial radii $x_k = R_k/R$, the normalized densities $\hat{d}_k = d_k/d_1$ for $k = 1, \ldots, 4$ and the quantity $f_4 = \int_0^1 \hat{d}(z) z^2 dz$. Finally, we use equations (6) and (7) of PI for $N = 4$ and take H_2 to bound the interior and

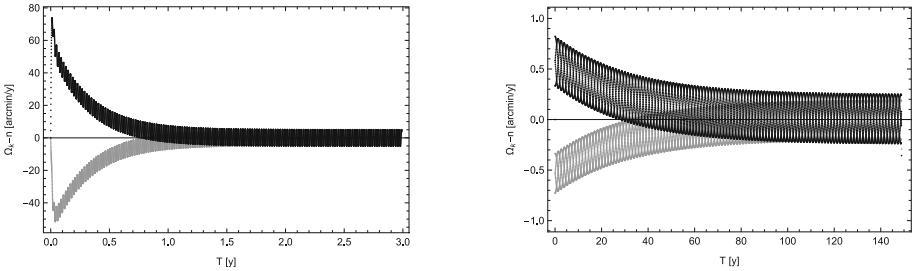

Fig. 7 Rotational evolution of $\Omega_k - n$ for different values for relaxation factors γ_c, γ_s: reference values on the left and small values on the right. Core ($k = c$) in gray and shell ($k = s$) in black

H_4 to bound the exterior: $H_c = H_2$ and $H_s = H_4$. The axial moment of inertia of the core (C_c) and the shell (C_s) is calculated again under the assumption of a four-layer structure: denoting by C_1, C_2, C_3, C_4 the polar moments of inertia of the four different layers (assumed to be spherical) we use $C_k = \frac{8}{15}\pi\rho_k(R_k^5 - R_{k-1}^5)$. To obtain C_c, C_s we calculate their sums according to $C_c = C_1 + C_2$, $C_s = C_3 + C_4$ by linearity of the integral forms. The equatorial flattening (tidal) is obtained from $\epsilon_k = H_k\bar{\epsilon}_\rho$ and (15) of PI to calculate $\bar{\epsilon}_\rho$ (following the same argumentation as below Table 4 in PI), where we take the mass of Jupiter M, the mass of Ganymede m_T and the semi-major axis a_{orb} again from Table 1. The relative heights of the elastic tides are assumed to be equal ($\lambda_c = \lambda_s$, following the comment in PI) and are obtained using equation (55) in PI: $\lambda_s = \frac{\epsilon_s'}{H_s\bar{\epsilon}_\rho} - 1$. Here, the equatorial prolateness is given by the formula $\epsilon_s' = \frac{a-b}{\sqrt{ab}}$, where a and b represent the equatorial semi-major axes of Ganymede (taken from 1). A relaxation factor γ (we omit the indices) can be related to the ratio $\frac{k_2}{Q}$ using equation (47) found in Ferraz-Mello (2013) by $\frac{25}{28}k_f(\frac{n}{\gamma} + \frac{\gamma}{n})$, where k_f is the fluid Love number that describes the deformability of the layer, according to (34) in Folonier et al. (2015): $k_f = \frac{5}{2}H - 1$. E.g., to calculate the relaxation factor γ_c we use n, k_{2i}, Q_{2i} from Table 1 and the Clairaut number H_c from Table 3 (and in an analogous way for γ_s). The remaining parameters are provided in Table 1 and 4: the Ganymede's tidal parameter τ is given by equation (47) in PI: $\tau = \frac{3n^2\bar{\epsilon}_\rho}{2}$, the friction parameter μ is defined in equation (53) in PI: $\mu = \frac{8\pi\eta_o R_c^4}{3h_o}$, which is λ_v defined in (15). Finally, the gravitational coupling constant can be calculated by equation (51) of PI that can be related to k_g in (14) (see appendix C).
The evolution of $\Omega_c - n$ and $\Omega_s - n$ for the parameters of Ganymede is shown in Fig. 7a. For relaxation factors γ_c, γ_s of the order 10^{-8} taken from Table 3 the (relaxation) damping time scales of the viscous layers turn out to be of the order 150 days. In Fig. 7b we show the dynamics based on the EDL model for the same parameters and initial conditions, but for relaxation factors of the order of 10^{-10}. As expected (see, e.g., Folonier and Ferraz-Mello 2017) the damping time scales increase (about 30 years, approximately by a factor 100, approaching the value obtained in Fig. 5a and b). It is interesting to discuss the difference between the dynamics based on the RDL and EDL models. In the RDL model the rigid layers oscillate around a nonzero value with nonzero amplitudes as shown in Fig. 5. The (tidal) damping time scales are of the order of 100 years for the reference parameters of Ganymede (bottom left panel) and are of the order of 3 years for k_2/Q increased by a factor 50 (bottom right panel). In comparison, the EDL model shows that the (relaxation) damping time scales of the viscous layers are of the order of 0.5 years (left of Fig. 7) and 30 years for smaller relaxation time (right panel). It is thus possible to fine-tune the tidal parameters in

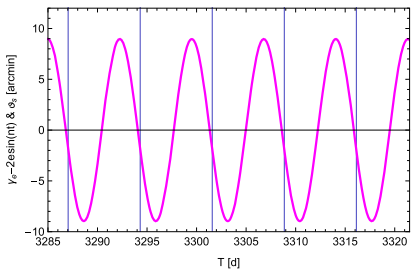

(a) Evolution of ϑ_s (in black) compared with the solution $\gamma_e - 2e \sin nt$ of the VTDL model (in magenta).

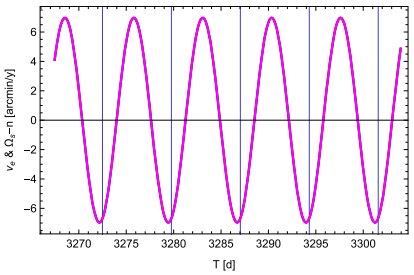

(b) Evolution of $\Omega_s - n$ (in black) compared with the solution v_e from the VTDL model (in magenta) after.

Fig. 8 Damped phase

the RDL model as well as the relaxation parameters of the EDL model to become of the same order of magnitudes. Since both parameters are linked to the same rheological parameters of the planetary moon, a comparative study of the RDL and EDL model might provide further insight into the internal properties of the moon also. Another obvious difference betweem the RDL and EDL dynamics is as follows. While during the damping phase in the RDL model both, the interior and the exterior are oscillating around a value close to zero, in the EDL model the core and the shell are oscillating in opposite phase with respect to each other with slightly larger excursions in amplitudes ($80 arcmin/y$ for the shell vs. $40 arcmin/y$ for the core). In the damped phase, however, the two signals tend to oscillate around zero with a period related to the orbital period of Ganymede around Jupiter (about 7.2 days).

We compare the damped phases of the RDL (VTDL) and EDL models in Fig. 8. The plots show the two signals in terms of angles and velocities for about 35 days. To make the comparison easier we have chosen same initial phases by shifting the two signals. In Fig. 8a we see the damped evolution of the angles: $\gamma_e - 2e \sin nt$ based on VTDL model (in magenta) and θ_s based on the EDL model (in black). As we can see the signals are in agreement both in terms of amplitude and period. As expected, the latter correspond to the Ganymede's orbital period, indicated by the background vertical blue lines. In Fig. 8b we see the damped evolution of the velocities: v_e based on VTDL model (in magenta) and $\Omega_s - n$ based on the EDL model (in black). As we can see the signal is also in good agreement in terms of the period. The center of oscillation is the same for both signals and corresponds to the exact spin-orbit resonance; the amplitude of the oscillations around the equilibrium is of the same order of magnitude, with a difference of about $1 arcmin/y$. The interior has similar behaviors, not shown here. We notice that the VTDL model reproduces the damped phases of both the RDL and EDL model with high accuracy.

4 Summary & conclusions

We start to investigate the rotational dynamics for the planetary moon Ganymede being situated in a spin-orbit resonance with planet Jupiter (in the so-called RDL model that is based on rigid layers). The moon is modeled by a thin external shell and an inner solid part, separated by a potential internal ocean. The focus of our study is on the amplitudes, periods and the damping time scales of the free librations around the exact spin-orbit resonance of the interior and exterior layers. In addition, we investigate the relaxation time scales of the deformable layers and compare the time scales and amplitudes with the former based on an alternative

dynamical model (EDL model based on elastic layers). We investigate and compare the separate effects of viscous coupling, tidal coupling and gravitational coupling, analyzing these effects on both isolated and coupled layers. In particular we provide dependencies on the parameters of the evolution of the oscillations on different time scales (e.g., see Figs. 4 to 5). We derive the nonlinear form of the equations of motion (RDL) from first principles for the two coupled resonant angles, one resonant angle for the interior and the other for the exterior. Additionally, we derive explicit solutions for linearized, single- and double-layer models (VTDL model), by using small angle approximations. These expressions allow us to analyze parameter dependencies and reproduce the dynamical evolution of libration angles with high accuracy.

Our findings allow us to predict the periods and amplitudes of time signals on different time scales. We provide a reference analytical model that accurately reproduces numerical signals. Moreover, we provide a reference set of parameters that are constrained by our model and current parameter values published in the recent literature. As it is shown the qualitative dynamics in the RDL, VTDL and EDL models have corresponding dynamical phases: after a transient time, the initial state (depending on initial conditions) is damped and the dynamics is dominated by the forced solution. From the solution of the VTDL model, which has the advantage to keep its dependency on the parameters, we summarize the following results (validated by numerical simulations based on the RDL model). The amplitudes of the free oscillations of both interior and exterior are of the order of $0.5\,acrmin$, corresponding to hundreds of meters on the surface of the body; the free periods of the exterior and interior are of the order of $0.5\,y$. Starting close to exact resonant initial conditions for the angles, and for reference values of Ganymede's parameters, the free oscillations are damped after about $100\,y$ (estimates obtained from VTDL model, confirmed by numerical simulations in the RDL model). We show that these damping time scales strongly depend on the tidal coefficients $\lambda_{ti}, \lambda_{te}$ (increasing the tidal coefficients the damping time scales decrease). Using the alternative model (EDL) we are also able to investigate the deformability of the different layers due to tidal interactions with Jupiter. While the damping in the RDL model refers to the time to synchronize the system the tidal damping in the EDL model refers to the relaxation time scale of the deformable layers that are needed to reach the equilibrium figures for the different layers. Typically, the relaxation time scales are found to be shorter than the tidal damping time (about a factor 100). For the system parameters of Ganymede and an initial offset from exact resonance of about $15\,arcmin$ the relaxation time turns out to be about $0.5\,y$. The time increases for smaller values of the relaxation factors, e.g., dividing the γ_c, γ_s by a factor 100 increases the relaxation time to about $30\,y$. It is interesting to study the parameters (λ_{tk}, γ_k) that are linked to the rheological properties of the moon and provide their ranges of values for which the time scales become comparable. For example, increasing the tidal coefficients in the RDL model by a factor 50, and/or decreasing the relaxation factors in the EDL model by 100, we get a damping time scale comparable to the relaxation time scale of the order of $3 - 30\,y$, respectively.

A comparison between the damped phases in the different models is interesting because they can be investigated by JUICE spacecraft. In the VTDL model the libration amplitudes of the final state (γ_i and γ_e) are explicitly given, while in the EDL model these informations are implicit in the angles θ_c and θ_s. As it is shown, the relations between these angles are $\theta_c = \gamma_i - 2e \sin nt$ (and similarly for the shell/exterior layer). From Fig. 8a it is clear that the damped regime predicted by the two models is the same in terms of amplitude and period. Their numerical values are the following. The interior has an amplitude of about $5 \cdot 10^{-6} \simeq 0.02\,arcmin$, corresponding to about $15\,m$, while the exterior has an amplitude of $6.5 \cdot 10^{-6} \simeq 0.025\,arcmin$, corresponding to about $20\,m$ on the surface of the layers. The

frequencies of both are equal to the mean motion, which is $n = 315.58\, y^{-1}$. The center of these forced oscillations is around $8 \cdot 10^{-4}\, arcmin$ for the interior and around $2 \cdot 10^{-3}\, arcmin$ for the exterior. These numbers are based on the actual parameters that are found in literature; once new measurements from the JUICE mission are available, the numbers will be updated. Both dynamical models that we use are complementary and highlight specific aspects of the real moon. Future studies on the long-term dynamics should focus on more sophisticated models of the interior structure of the moon and the orbital interactions with the other planetary moons.

A Derivation of the viscous coefficient

In a point on the IEB (Interior-Exterior-Boundary) at a distance r with respect to the rotational axis, the relative tangential velocity is $v_{rel} = r\omega_{rel} = r(\dot{\gamma}_i - \dot{\gamma}_e)$. Assuming a laminar regime for the ocean, it is possible to define its viscosity:

$$\eta_o = \frac{f_v h}{v_{rel}}, \tag{56}$$

where f_v is the viscous force per unit surface acting on the IEB and h is the ocean's thickness. The viscous torque per unit surface acting on the IEB with respect to the rotational axis is $r f_v$, and then the total torque is obtained integrating this unit torque over all the IEB surface:

$$\begin{aligned} T_v &= \int_\Sigma f_v\, r\, d\sigma = \int_0^{2\pi} \int_0^{\pi} \frac{\eta_o\, v_{rel}}{h}\, r\, R^2\, \sin\vartheta\, d\vartheta\, d\phi \\ &= \int_0^{2\pi} \int_0^{\pi} \frac{\eta_o\, \omega_{rel}}{h}\, r^2\, R^2\, \sin\vartheta\, d\vartheta\, d\phi. \end{aligned} \tag{57}$$

Since $r = R_i \sin\vartheta$ is the distance between the rotational axis (z axis) and the point of geographic coordinate (ϕ, ϑ) on the IEB we have:

$$T_v = 2\pi \frac{\eta_o \omega_{rel} R_i^4}{h} \int_0^{\pi} \sin^3\vartheta d\vartheta = \frac{8\pi}{3} \frac{\eta_o R_i^4 (\dot{\gamma}_i - \dot{\gamma}_e)}{h} = \lambda_v (\dot{\gamma}_i - \dot{\gamma}_e). \tag{58}$$

Hence the viscous coupling coefficient is given by:

$$\lambda_v = \frac{8\pi}{3} \frac{\eta_o R_i^4}{h}, \tag{59}$$

that is equation (53) in Folonier and Ferraz-Mello (2017).

B Derivation of the tidal coefficients

The potential of a homogeneous body in an external point P at a distance r from the center of the body is given by equation (4.54) in Murray and Dermott (1999):

$$V_0(r; \theta, R, \rho, \epsilon_2) = -\frac{4}{3}\pi R^3 \rho G \left[\frac{1}{r} + \frac{3}{5} \frac{R^2}{r^3} \epsilon_2 P_2(\cos\theta) \right], \tag{60}$$

where G is the gravitational constant, ρ the density of the body, R its mean radius, $\epsilon_2 << 1$ its equatorial flattening, P_2 the second-degree Legendre polynomial and θ is the angle between the position of P and the semimajor axis of the body (i.e., the tidal bulges).

We can compute the potential in a point P due to a body made of two layer of different densities ρ_i and ρ_e by first considering the body as it was homogeneous of density ρ_e and then replace an internal portion of radius R_i, flattening ϵ_{2i} and oriented with an angle θ_i, with a material of density ρ_i. Thus, we obtain:

$$V(r;\theta_i,\theta_e,R_i,R_e\rho_i,\rho_e,\epsilon_{2i},\epsilon_{2e}) = V_0(r;\theta_e,R_e,\rho_e,\epsilon_{2e}) - V_0(r;\theta_i,R_i,\rho_e,\epsilon_{2i}) + V_0(r;\theta,R_i,\rho_i,\epsilon_{2i}). \tag{61}$$

The relation between the flattening ϵ_2 and the static Love number k_2 can be obtained from equations (4.154) and (4.156) in Murray and Dermott (1999), namely:

$$\epsilon_{2i} = \frac{5}{3}\frac{\zeta_i}{R_i}k_{2i} \quad \text{and} \quad \epsilon_{2e} = \frac{5}{3}\frac{\zeta_e}{R_e}k_{2e}, \tag{62}$$

where

$$\zeta_i = \frac{M}{m_i}\left(\frac{R_i}{r}\right)^3 R_i \quad \text{and} \quad \zeta_e = \frac{M}{m_e}\left(\frac{R_e}{r}\right)^3 R_e \tag{63}$$

are the maximal tidal heights of interior and exterior, respectively, due to a tide raising body placed at a distance r.
Finally, using (62), (63) and replacing $m_i = \frac{4}{3}\pi R_i^3\rho_i$ and $m_e = \frac{4}{3}\pi(R_e^3 - R_i^3)\rho_e$ (that means assuming spherical objects to calculate the masses), the potential (61) becomes:

$$V(r,\theta_i,\theta_e) = -\frac{4}{3}\pi R_e^3\rho_e G\left[\frac{1}{r} + \frac{3K_{2e}MR_e^5(3\cos^2\theta_e - 1)}{8\pi r^6(R_e^3 - R_i^3)\rho_e}\right] - \frac{4}{3}\pi R_i^3(\rho_i - \rho_e)G\left[\frac{1}{r} + \frac{3K_{2i}MR_i^2(3\cos^2\theta_i - 1)}{8\pi r^6\rho_i}\right]. \tag{64}$$

The torques due to the interior and exterior layers acting on the tide raising planet of mass M placed in $\mathbf{r}$ are:

$$\begin{aligned}\Gamma_i &= -M\frac{\partial V(r,\theta_i,\theta_e)}{\partial\theta_i} = -\frac{3Gk_{2i}M^2R_i^5}{r^6}\frac{\rho_i - \rho_e}{\rho_i}\sin\theta_i\cos\theta_i,\\ \Gamma_e &= -M\frac{\partial V(r,\theta_i,\theta_e)}{\partial\theta_e} = -\frac{3Gk_{2e}M^2R_e^5}{r^6}\frac{R_e^3}{[R_e^3 - (R_e - h_e)^3]}\sin\theta_e\cos\theta_e,\end{aligned} \tag{65}$$

where we have introduced the exterior thickness $h_e = R_e - R_i$.
From Newton's laws of motion it follows that the torque acting on the interior and on the exterior layers is equal and opposite to those given in equation (65).
It is possible to reduce Γ_i and Γ_e to have the same form by introducing two dimensionless factors f_i and f_e, defined as:

$$f_i = \frac{\rho_i - \rho_e}{\rho_i} \quad \text{and} \quad f_e = \frac{R_e^3}{[R_e^3 - (R_e - h_e)^3]}. \tag{66}$$

Hence, we obtain the form given by equation (16) in Peale (2005):

$$\begin{aligned}\mathbf{\Gamma_{ti}} &= \frac{3GM^2f_ik_{2i}R_i^5}{a^6}\left(\frac{a}{r}\right)^6(\hat{\mathbf{r}}\cdot\hat{\mathbf{r}}_\mathbf{i})(\hat{\mathbf{r}}\times\hat{\mathbf{r}}_\mathbf{i}),\\ \mathbf{\Gamma_{te}} &= \frac{3GM^2f_ek_{2e}R_e^5}{a^6}\left(\frac{a}{r}\right)^6(\hat{\mathbf{r}}\cdot\hat{\mathbf{r}}_\mathbf{e})(\hat{\mathbf{r}}\times\hat{\mathbf{r}}_\mathbf{e}),\end{aligned} \tag{67}$$

where $\hat{\mathbf{r}}$ represents the unit vector toward the planet; $\hat{\mathbf{r}}_\mathbf{i}$ and $\hat{\mathbf{r}}_\mathbf{e}$ are the unit vector toward the tidal maximum of the interior or the exterior layer, respectively.
Following the steps shown in Peale (2005), it is possible to obtain the expression of the averaged z component of the tidal torque acting on a satellite in 1 : 1 spin-orbit resonance up to the second order in the eccentricity that enters equation (13):

$$\langle \Gamma_{ti,z} \rangle = \lambda_{ti} \left(\langle \dot{\gamma}_i \rangle - 6ne^2 \right) \quad \text{and} \quad \langle \Gamma_{te,z} \rangle = \lambda_{te} \left(\langle \dot{\gamma}_e \rangle - 6ne^2 \right), \tag{68}$$

where λ_{ti} and λ_{te} are given in equation (16).

C Notes on the derivation of the gravitational coefficient

We provide some details on the derivation of k_g, see, e.g., Szeto and Xu (1997) and Coyette et al. (2016) for further details. The expression of the gravitational potential due to a triaxial ellipsoidal shell in a point $\vec{r}$ (inside or outside the ellipsoidal cavity) is given in equation (5a) in Szeto and Xu (1997):

$$\Phi(\vec{r}) = \alpha + \beta r^2 P_2(\cos\theta) + \gamma r^2 P_2^2(\cos\theta)\cos 2\phi, \tag{69}$$

with:

$$\begin{aligned}
\alpha &= 2\pi\rho G \left[a_2^2 \left(1 - \frac{2}{3} f_2 - \frac{f_2^2}{5} - \frac{2}{3} k_2 \right) - a_1^2 \left(1 - \frac{2}{3} f_1 - \frac{f_1^2}{5} - \frac{2}{3} k_1 \right) \right] \\
\beta &= \frac{4}{5}\pi\rho G \left[-\frac{2}{3}(f_2 - f_1) + \frac{1}{3}(k_2 - k_1) - \frac{3}{7}(f_2^2 - f_1^2) \right] \\
\gamma &= \frac{2}{15}\pi\rho G (k_2 - k_1).
\end{aligned} \tag{70}$$

These expressions are valid up to the first order in the equatorial flattening $k = \frac{a-b}{a}$ and up to the second order in the polar flattening $f = \frac{a-c}{a}$, respectively. They are obtained considering separately the contributions inside and outside the ellipsoidal cavity (see e.g., Figure A1 in Szeto and Xu 1997) and expanding the integrals in spherical harmonics. To solve these integrals the cases $l > 2$, $l = 2$, $l = 1$ and $l = 0$ are considered separately. In each case, first the integral in the variable r is solved. Then the radii are expressed in terms of colatitude θ and longitude ϕ up to the first order in the equatorial flattening k and up to the second order in the flattening f. Finally the remaining integrals are solved by using the orthogonality properties of spherical harmonics.
In Cartesian coordinates, equation (69) becomes:

$$\Phi = \alpha + \left(3\gamma - \frac{1}{2}\beta \right) x^2 + \left(-3\gamma - \frac{1}{2}\beta \right) y^2 + \beta z^2, \tag{71}$$

that is expressed in the BF of the interior layer. In order to find its expression in the BF of the exterior layer we have to perform a suitable transformation. First, we describe the form of the torque under a generic transformation (parametrized by l's, m's, n's coefficients, see below). Next, we consider the particular transformation that we need to find the desired expression. The third component of the gravitational torque per unit volume and per unit mass acting on a point of the interior shell is: $d\Gamma_{g,z} = X\partial_y\Phi - Y\partial_x\Phi$. The torque $\Gamma_{g,z}$ is obtained by integrating $\rho_i d\Gamma_{g,z}$ over all the interior's volume:

$$\Gamma_{g,z} = \left[\gamma \left(6l_1 l_2 - 6m_1 m_2 \right) + \beta \left(2n_1 n_2 - l_1 l_2 - m_1 m_2 \right) \right] (B_i - A_i), \tag{72}$$

where $A_i = \int (Y^2 + Z^2) dm$ and $B_i = \int (X^2 + Z^2) dm$ are the principal moments of inertia of the interior shell with respect to the X and the Y axes, respectively. Assuming the planar approximation, the transformation from interior BF to exterior BF is just a rotation by an angle $(\gamma_e - \gamma_i)$ around the z axis:

$$R = \begin{pmatrix} l_1 & l_2 & l_3 \\ m_1 & m_2 & m_3 \\ n_1 & n_2 & n_3 \end{pmatrix} = \begin{pmatrix} 1 & \gamma_e - \gamma_i & 0 \\ -(\gamma_e - \gamma_i) & 1 & 0 \\ 0 & 0 & 1 \end{pmatrix}. \tag{73}$$

Substituting these expressions for the $l's$, $m's$ and $n's$ coefficients into the expression (72), we obtain the form of the third component of the gravitational torque:

$$\Gamma_{g,z} = 12\gamma(\gamma_e - \gamma_i)(B_i - A_i). \tag{74}$$

Finally γ is given in (70), but we consider a more generalize expression that allows the possibility of an exterior made of layers with different densities:

$$\gamma = \frac{2}{15}\pi G \int_{r_1}^{r_2} \rho(r) \frac{\partial k(r)}{\partial r} dr = \frac{2}{15}\pi G[\rho_o k_o + \rho_s(k_s - k_o)]. \tag{75}$$

Here, we have considered the exterior made of two layers with different densities: a liquid ocean (o) and an icy shell (s). The interior ocean's surface is assumed to be spherical $k_{o,int} = 0$, the exterior ocean's surface coincides with the interior shell's surface $k_{o,ext} = k_{s,int} = k_o$ and the exterior shell's surface is the exterior body's surface $k_{s,ext} = k_s$, as in Fig.2. Therefore the expression for the z-component of the gravitational torque is:

$$\Gamma_{g,z} = \frac{8}{5}\pi G(B_i - A_i)\left[\rho_o k_o + \rho_s(k_s - k_o)\right](\gamma_e - \gamma_i) = k_g(\gamma_e - \gamma_i), \tag{76}$$

with the gravitational coupling constant k_g given by:

$$k_g = \frac{8}{5}\pi G(B_i - A_i)\left[\rho_s(k_s - k_o) + \rho_o k_o\right], \tag{77}$$

that is equation (14) by replacing symbol k with β. To compare this expression with (51) of PI, we have to assume that the exterior layer is homogeneous (this can be done by setting $k_o = 0$) and by taking the half of k_g, see (13) and (54):

$$k_i = \frac{4}{5}\pi G(B_{int} - A_{int})\rho_s k_s. \tag{78}$$

Equations (78) and (51) of PI are the same if the terms $\frac{4}{5}(B_{int} - A_{int})$ and $\frac{32}{75}\pi\epsilon_c' d_c R_c^5$ are equal (since k_s and ϵ_s' refer both to the equatorial flattenings). Rewriting both the expressions in a different form, omitting the subscripts since they refer to the interior (core) only, we get:

$$\frac{4}{5}(B - A) = \frac{4}{5}\left[\frac{1}{5}m(a^2 + c^2) - \frac{1}{5}m(b^2 + c^2)\right] = \frac{4}{5}\frac{1}{5}m(a^2 - b^2) = \frac{4}{25}m(a^2 - b^2) \tag{79}$$

and

$$\frac{32}{75}\pi\epsilon' d R^5 = \frac{32}{75}\pi\frac{a-b}{R}\frac{m}{V}R^5 = \frac{24}{75}m(a-b)R = \frac{12}{75}m(a-b)(a+b) = \frac{4}{25}m(a^2 - b^2). \tag{80}$$

Here, we have considered a sphere $V = \frac{4}{3}\pi R^3$ and expressed the mean equatorial radius as $R = (a + b)/2$. This shows that the two expressions for the gravitational coupling constant are equivalent.

D Approximate expressions

Expressions for the real parts of the eigenvalues, VDL, TDL model

Approximate expressions for the real parts of the eigenvalues in the VDL and TDL cases are found by searching for solutions of the characteristic polynomials of the form $x = \delta_r + \mathrm{j}(x + \delta_i)$ and solving for δ_r. In the VDL case we obtain:

$$-\frac{\lambda_v\left(C_e\left(2C_i k_g\left(-\omega_i^2\left(\omega_e^2+x^2\right)-x^2\omega_e^2+3x^4\right)+C_i^2\left(\omega_e^2+x^2\right)\left(x^2-\omega_i^2\right)^2+k_g^2\left(3x^2-\omega_e^2\right)\right)+C_e^2 C_i\left(x^2-\omega_e^2\right)^2\left(\omega_i^2+x^2\right)+k_g^2\left(C_i\left(3x^2-\omega_i^2\right)+2k_g\right)\right)}{2C_e\lambda_v^2\left(3x^2-\omega_e^2\right)\left(C_i\left(3x^2-\omega_i^2\right)+2k_g\right)+C_e^2\left(4x^2C_i^2\left(\omega_e^2+\omega_i^2-2x^2\right)^2+\lambda_v^2\left(\omega_e^2-3x^2\right)^2\right)+\lambda_v^2\left(C_i\left(3x^2-\omega_i^2\right)+2k_g\right)^2} \tag{81}$$

In the TDL case we get:

$$-\frac{C_e\left(C_i^2\lambda_e\left(\omega_e^2+x^2\right)\left(x^2-\omega_i^2\right)^2+\lambda_i\left(k_g^2\left(3x^2-\omega_e^2\right)+x^2\lambda_e\lambda_i\left(\omega_e^2+x^2\right)\right)\right)+C_i\lambda_e\left(x^2\lambda_e\lambda_i\left(\omega_i^2+x^2\right)+k_g^2\left(3x^2-\omega_e^2\right)\right)+C_e^2C_i\lambda_i\left(x^2-\omega_e^2\right)^2\left(\omega_i^2+x^2\right)}{C_e^2\left(4x^2C_i^2\left(\omega_e^2+\omega_i^2-2x^2\right)^2+\lambda_i^2\left(\omega_e^2-3x^2\right)^2\right)+2C_eC_i\lambda_e\lambda_i\left(\omega_e^2+x^2\right)\left(\omega_i^2+x^2\right)+\lambda_e^2\left(C_i^2\left(\omega_i^2-3x^2\right)^2+4x^2\lambda_i^2\right)} \tag{82}$$

In these expressions one has to replace x with ω_{0i} or ω_{0e} to obtain the damping time scales for the interior or the exterior, respectively. For the VDL case (YRM units): $\tau_{1,2} = -2.299\cdot 10^{-9}$, $\tau_{3,4} = -1.032\cdot 10^{-10}$; for the TDL case: $\tau_{1,2} = -1.212\cdot 10^{-12}$, $\tau_{3,4} = -6.104\cdot 10^{-12}$. These values should be compared with those obtained numerically from (24).

Expressions of the initial condition-dependent coefficients for the CDL model

The expressions of the initial condition-dependent constant c_1, c_2, c_3, c_4 that we obtain for the CDL model are:

$$\begin{aligned}
c_{1,2} =& -\frac{2k_g^3v_{0i}+3C_sk_g^2v_{0e}\left(\omega_{0e}^2-\omega_{0i}^2\right)-C_sC_ik_gv_{0i}\left(\omega_{0e}^2-\omega_{0i}^2\right)^2+C_s^2C_iv_{0e}\left(\omega_{0e}^2-\omega_{0i}^2\right)^3}{2C_s\left(\omega_{0e}^2-\omega_{0i}^2\right)\left[4k_g^2+C_sC_i\left(\omega_{0e}^2-\omega_{0i}^2\right)^2\right]}\\
&\pm\mathrm{j}\frac{\left[k_g^2+2C_sC_i\omega_{0e}\left(\omega_{0e}^2-\omega_{0i}^2\right)\right]\left[2k_g^3\gamma_{0i}+C_sC_ik_g\gamma_{0i}\left(\omega_{0e}^2-\omega_{0i}^2\right)^2-C_s^2C_i\gamma_{0e}\left(\omega_{0e}^2-\omega_{0i}^2\right)^3-3C_sk_g^3\gamma_{0e}\left(\omega_{0e}^2-\omega_{0i}^2\right)\right]}{4C_s^2C_i\omega_{0e}\left(\omega_{0e}^2-\omega_{0i}^2\right)^2\left[4k_g^2+C_sC_i\left(\omega_{0e}^2-\omega_{0i}^2\right)^2\right]}\\
c_{3,4} =& -\frac{2k_g^3v_{0i}+3C_sk_g^2v_{0e}\left(\omega_{0e}^2-\omega_{0i}^2\right)-C_sC_ik_gv_{0i}\left(\omega_{0e}^2-\omega_{0i}^2\right)^2}{2C_s\left(\omega_{0e}^2-\omega_{0i}^2\right)\left[4k_g^2+C_sC_i\left(\omega_{0e}^2-\omega_{0i}^2\right)^2\right]}\\
&\pm\mathrm{j}\frac{\left[2k_g^3\gamma_{0i}+2C_sk_g^2\gamma_{0e}\left(\omega_{0e}^2-\omega_{0i}^2\right)+C_sC_i\gamma_{0i}\left(\omega_{0e}^2-\omega_{0i}^2\right)^2\right]\left[k_g^2-2C_sC_i\omega_{0i}\gamma_{0i}^2\left(\omega_{0e}^2-\omega_{0i}^2\right)\right]}{4C_s^2C_i\omega_{0i}\left(\omega_{0e}^2-\omega_{0i}^2\right)^2\left[4k_g^2+C_sC_i\left(\omega_{0e}^2-\omega_{0i}^2\right)^2\right]}
\end{aligned} \tag{83}$$

Acknowledgements CL acknowledges the support of the Italian MIUR Department of Excellence grant MatMod@TOV 2023-2027 (CUP E83C23000330006). GP, MV have been supported through the ASI Contract n.2023-6-HH.0, Scientific Activities for JUICE, E phase (CUP F83C23000070005). The authors would like to thank A. Celletti, B. Scoppola, S. Ferraz-Mello and the Radio Science Laboratory (Sapienza University of Rome) for insightful discussions and valuable comments on the topic.

Author Contributions The authors contributed equally to the work

Funding Open access funding provided by Università degli Studi di Roma Tor Vergata within the CRUI-CARE Agreement.

Data Availability No datasets were generated or analyzed during the current study.

Declarations

Conflict of interest The authors declare no conflict of interest.

References

Lari, G., Saillenfest, M.: The nature of the Laplace resonance between the Galilean moons. CMDA **136**(3), 19 (2024). https://doi.org/10.1007/s10569-024-10191-6

Celletti, A., Karampotsiou, E., Lhotka, C., Pucacco, G., Volpi, M.: Laplace-like resonances with tidal effects. A&A **655**, A94 (2021). https://doi.org/10.1051/0004-6361/202141311

Lari, G., Saillenfest, M., Fenucci, M.: Long-term evolution of the Galilean satellites: the capture of Callisto into resonance. A&A **639**, A40 (2020). https://doi.org/10.1051/0004-6361/202037445

Tobie, G., Auclair-Desrotour, P., Běhounková, M., Kervazo, M., Souček, O., Kalousová, K.: Tidal deformation and dissipation processes in Icy worlds. Space Sci. Rev. **221**(1), 6 (2025). https://doi.org/10.1007/s11214-025-01136-y

Spohn, T., Schubert, G.: Oceans in the icy Galilean satellites of Jupiter? Icarus **161**(2), 456–467 (2003). https://doi.org/10.1016/S0019-1035(02)00048-9. (**ISSN 0019-1035**)

Šachl, L., Kvorka, J., Čadek, O., Velímský, J.: Magnetic field induced by convective flow in Europa's subsurface ocean. Icarus **429**, 116375 (2025). https://doi.org/10.1016/j.icarus.2024.116375

Kaweeyanun, N., Masters, A.: Three-dimensional modeling of Ganymede's Chapman-Ferraro magnetic field and its role in subsurface ocean induction. Icarus **426**, 116356 (2025). https://doi.org/10.1016/j.icarus.2024.116356

De Marchi, F., Cappuccio, P., Mitri, G., Iess, L.: Frequency-dependent Ganymede's tidal Love number k_2 detection by JUICE's 3GM experiment and implications for the subsurface ocean thickness. Icarus **386**, 115150 (2022). https://doi.org/10.1016/j.icarus.2022.115150

Tobie, G., Grasset, O., Dumoulin, C., Mocquet, A.: Tidal response of rocky and ice-rich exoplanets. Astron. Astrophys. **630**, A70 (2019)

William, B.M., Schubert, G.: The tidal response of Ganymede and Callisto with and without liquid water oceans. Icarus **166**(1), 223–226 (2003). https://doi.org/10.1016/j.icarus.2003.07.001. (**ISSN 0019-1035**)

Kivelson, M.G., Khurana, K.K., Volwerk, M.: The permanent and inductive magnetic moments of Ganymede. Icarus **157**(2), 507–522 (2002)

Kaweeyanun, N., Masters, A.: Three-dimensional modeling of Ganymede's Chapman-Ferraro magnetic field and its role in subsurface ocean induction. Icarus **426**, 116356 (2025)

Jia, X., Kivelson, M.G., Khurana, K.K., Walker, R.J.: Improved models of Ganymede's permanent and induced magnetic fields based on Galileo and Juno data. J. Geophys. Res.: Planets **130**(1), e2024JE008309 (2025)

Roberts, J.H., McKinnon, W.B., Elder, C.M., Tobie, G., Biersteker, J.B., Young, D., Park, R.S., Steinbrügge, G., Nimmo, F., Howell, S.M., Castillo-Rogez, J.C., Cable, M.L., Abrahams, J.N., Bland, M.T., Chivers, C., Cochrane, C.J., Dombard, A.J., Ernst, C., Genova, A., Gerekos, C., Glein, C., Harris, C.D., Hay, H., Hayne, P.O., Hedman, M., Hussmann, H., Jia, X., Khurana, K., Kiefer, W.S., Kirk, R., Kivelson, M., Lawrence, J., Leonard, E.J., Lunine, J.I., Mazarico, E., McCord, T.B., McEwen, A., Paty, C., Quick, L.C., Raymond, C.A., Retherford, K.D., Roth, L., Rymer, A., Saur, J., Scanlan, K., Schroeder, D.M., Senske, D.A., Shao, W., Soderlund, K., Spiers, E., Styczinski, M.J., Tortora, P., Vance, S.D., Villarreal, M.N., Weiss, B.P., Westlake, J.H., Withers, P., Wolfenbarger, N., Buratti, B., Korth, H., Pappalardo, R.T.: The Interior Thematic Working Group. Exploring the Interior of Europa with the Europa Clipper. Space Science Reviews **219**(6), 46 (2023). https://doi.org/10.1007/s11214-023-00990-y

Van Hoolst, T., Tobie, G., Vallat, C., Altobelli, N., Bruzzone, L., Cao, H., Dirkx, D., Genova, A., Hussmann, H., Iess, L., Kimura, J., Khurana, K., Lucchetti, A., Mitri, G., Moore, W., Saur, J., Stark, A., Vorburger, A., Wieczorek, M., Aboudan, A., Bergman, J., Bovolo, F., Breuer, D., Cappuccio, P., Carrer, L., Cecconi, B., Choblet, G., De Marchi, F., Fayolle, M., Fienga, A., Futaana, Y., Hauber, E., Kofman, W., Kumamoto, A., Lainey, V., Molyneux, P., Mousis, O., Plaut, J., Puccio, W., Retherford, K., Roth, L., Seignovert, B., Steinbrügge, G., Thakur, S., Tortora, P., Tosi, F., Zannoni, M., Barabash, S., Dougherty, M., Gladstone, R., Gurvits, L.I., Hartogh, P., Palumbo, P., Poulet, F., Wahlund, J.E., Grasset, O., Witasse, O.: Geophysical Characterization of the Interiors of Ganymede, Callisto and Europa by ESA's JUpiter ICy moons Explorer. Space Sci. Rev. **220**(5), 54 (2024). https://doi.org/10.1007/s11214-024-01085-y

Cappuccio, P., Sesta, A., Di Benedetto, M., Durante, D., De Filippis, U., di Stefano, I., Iess, L., Mackenzie, R., Godard, B.: Analysis of Radio Science Data from the KaT Instrument of the 3GM Experiment During JUICE's Early Cruise Phase. Aerospace **12**(1), 56 (2025). https://doi.org/10.3390/aerospace12010056

Cappuccio, P., Hickey, A., Durante, D., Di Benedetto, M., Iess, L., De Marchi, F., Plainaki, C., Milillo, A., Mura, A.: Ganymede's gravity, tides and rotational state from JUICE's 3GM experiment simulation. Planet. Space Sci. **187**, 104902 (2020)

De Marchi, F., Di Achille, G., Mitri, G., Cappuccio, P., Di Stefano, I., Iess, L. et al.: Observability of Ganymede's gravity anomalies related to surface features by the 3GM experiment onboard European Space Agency (ESA) JUpiter ICy moons Explorer (JUICE) mission. In: Libro degli abstract. XVI congresso nazionale di scienze planetarie, pp. 24–24, (2020)

Hussmann, H., Lingenauber, K., Stark, A., Enya, K., Thomas, N., Lara, L.M., Althaus, C., Araki, H., Behnke, T., Binger, J., et al.: The Ganymede Laser Altimeter (GALA) on the Jupiter Icy Moons Explorer (JUICE) Mission. Space Sci. Rev. **221**(3), 33 (2025)

Van Hoolst, T., Rambaux, N., Karatekin, O., Dehant, V., Rivoldini, A.: The librations, shape, and icy shell of Europa. Icarus **195**(1), 386–399 (2008)

Baland, R.M., Van Hoolst, T.: Librations of the Galilean satellites: The influence of global internal liquid layers. Icarus **209**(2), 651–664 (2010)

Van Hoolst, T., Baland, R., Trinh, A.: On the librations and tides of large icy satellites. Icarus **226**(1), 299–315 (2013). https://doi.org/10.1016/j.icarus.2013.05.036. (**ISSN 0019-1035**)

Furi, M., Martelli, M., Vignoli, A., et al.: Longitudinal librations of a satellite. Electron. J. Differential Equations **2011**(134), 1–15 (2011)

Burton, P.: Planar librations of an extensible dumbbell satellite. AIAA J. **1**(2), 411–418 (1963)

Scoppola, B., Troiani, A., Veglianti, M.: Tides and dumbbell dynamics. Regular Chaotic Dyn. **27**(3), 369–380 (2022)

Henrard, J., Schwanen, G.: Rotation of synchronous satellites application to the Galilean satellites. Celest. Mech. Dyn. Astron. **89**, 181–199 (2004)

Lhotka, C.: A symplectic mapping for the synchronous spin-orbit problem. Celest. Mech. Dyn. Astron. **115**(4), 405–426 (2013). https://doi.org/10.1007/s10569-012-9464-5

Lhotka, C.: Steady state obliquity of a rigid body in the spin-orbit resonant problem: application to Mercury. Celest. Mech. Dyn. Astron. **129**(4), 397–414 (2017). https://doi.org/10.1007/s10569-017-9787-3

Ragazzo, C., Boué, G., Gevorgyan, Y., Ruiz, L.S.: Librations of a body composed of a deformable mantle and a fluid core. Celest. Mech. Dyn. Astron. **134**(2), 10 (2022)

Noyelles, B.: Theory of the rotation of the Galilean satellites. Proc. Int. Astron. Union **6**(S269), 240–244 (2010)

Rambaux, N., Henrard, J.: The rotation of the galilean satellites in The rotation of celestial bodies In: Lemaıtre, A. (ed.) Presses Universitaires de Namur, Namur, Belgium, (2005)

Rambaux, N., Castillo-Rogez, J.C., Williams, J.G., Karatekin, O.: Librational response of Enceladus. Geophys. Res. Lett. (2010). https://doi.org/10.1029/2009GL041465

Van Hoolst, T., Baland, R., Trinh, A.: On the librations and tides of large icy satellites. Icarus **226**(1), 299–315 (2013). https://doi.org/10.1016/j.icarus.2013.05.036

Van Hoolst, T., Baland, R.M., Trinh, A., Yseboodt, M., Nimmo, F.: The Librations, Tides, and Interior Structure of Io. J. Geophys. Res. (Planets) **125**(8), e06473 (2020). https://doi.org/10.1029/2020JE006473

Folonier, H.A., Ferraz-Mello, S.: Tidal synchronization of an anelastic multi-layered body: Titan's synchronous rotation. Celest. Mech. Dyn. Astron. **129**, 359–396 (2017)

Folonier, H.A., Ferraz-Mello, S., Kholshevnikov, K.V.: The flattenings of the layers of rotating planets and satellites deformed by a tidal potential. Celest. Mech. Dyn. Astron. **122**(2), 183–198 (2015)

Ferraz-Mello, S.: Tidal synchronization of close-in satellites and exoplanets. A rheophysical approach. Celes. Mech. Dyn. Astron. **116**(2), 109–140 (2013)

Sansottera, M., Lhotka, C., Lemaitre, A.: Effective stability around the Cassini state in the spin-orbit problem. Celest. Mech. Dyn. Astron. **119**(1), 75–89 (2014). https://doi.org/10.1007/s10569-014-9547-6

Celletti, A., Lhotka, C.: Transient times, resonances and drifts of attractors in dissipative rotational dynamics. Commun. Nonlinear Sci. Numer. Simul. **19**(9), 3399–3411 (2014)
Lainey, V., Duriez, L., Vienne, A.: Synthetic representation of the Galilean satellites' orbital motions from L1 ephemerides. Astron. Astrophys. **456**(2), 783–788 (2006)
Bills, B.G.: Free and forced obliquities of the Galilean satellites of Jupiter. Icarus **175**(1), 233–247 (2005)
Rambaux, N., Van Hoolst, T., Karatekin, O.: Librational response of Europa, Ganymede, and Callisto with an ocean for a non-Keplerian orbit. Astron. Astrophys. **527**, A118 (2011)
Baland, R.M., Yseboodt, M., Van Hoolst, T.: Obliquity of the Galilean satellites: The influence of a global internal liquid layer. Icarus **220**(2), 435–448 (2012)
Peale, S.J.: Obliquity tides in hot Jupiters. Extreme Solar Syst. **398**, 281 (2008)
Coyette, A., Van Hoolst, T., Baland, R.M., Tokano, T.: Modeling the polar motion of Titan. Icarus **265**, 1–28 (2016)
Baland, R.M., Coyette, A., Van Hoolst, T.: Coupling between the spin precession and polar motion of a synchronously rotating satellite: application to Titan. Celest. Mech. Dyn. Astron. **131**, 1–50 (2019)
Casajus, L.G., Ermakov, A.I., Zannoni, M., Keane, J.T., Stevenson, D., Buccino, D.R., Durante, D., Parisi, M., Park, R.S., Tortora, P., et al.: Gravity field of ganymede after the juno extended mission. Geophys. Res. Lett. **49**(24), e2022GL099475 (2022)
Rochester, M.G.: Core-mantle interactions: geophysical and astronomical consequences. In Earthquake Displacement Fields and the Rotation of the Earth: A NATO Advanced Study Institute Conference Organized by the Department of Geophysics, University of Western Ontario, London, Canada, 22 June–28 June 1969, pages 136–148. Springer, (1970)
Correia, A.C.M., Laskar, J.: Mercury's capture into the 3/2 spin-orbit resonance including the effect of core-mantle friction. Icarus **201**(1), 1–11 (2009)
Murray, C.D., Dermott, S.F.: Solar system dynamics. Cambridge University Press, Cambridge (1999)
Efroimsky, M., Makarov, V.V.: Tidal friction and tidal lagging. Applicability limitations of a popular formula for the tidal torque. The Astrophys. J. **764**(1), 26 (2013)
Efroimsky, M.: Tidal evolution of asteroidal binaries. Ruled by viscosity. Ignorant of rigidity. The Astron. J. **150**(4), 98 (2015)
Ferraz-Mello, S., Grotta-Ragazzo, C., Dos Santos, L.R.: Dissipative forces in celestial mechanics. 30o Colóquio Brasileiro de Matemática. Publicaçoes Matemáticas, IMPA, (2015)
Peale, S.J.: The free precession and libration of Mercury. Icarus **178**(1), 4–18 (2005)
Pinzari, G., Scoppola, B., Veglianti, M.: Spin orbit resonance cascade via core shell model: Application to Mercury and Ganymede. Celest. Mech. Dyn. Astron. **136**(5), 1–20 (2024)
Jara-Orué, H.M., Vermeersen, B.L.A.: Tides on Jupiter's moon Ganymede and their relation to its internal structure. Neth. J. Geosci. **95**(2), 191–201 (2016)
Szeto, A.M.K., Xu, S.: Gravitational coupling in a triaxial ellipsoidal Earth. J. Geophys. Res.: Solid Earth **102**(B12), 27651–27657 (1997)